Markus Huber

Infrared Behavior of Vertex Functions in d-Dimensional Yang-Mills Theory

Diplomarbeit

zur Erlangung des Magistergrades der Naturwissenschaften

verfasst am Institut für Physik, Fachbereich Theoretische Physik an der Karl-Franzens-Universität Graz

Betreuer: Univ.-Prof. Dr. rer. nat. Reinhard Alkofer

Graz, 2007

Contents

1	Intro	oduction	5
2	Und	lerlying Physical Concepts	7
	2.1		7
		2.1.1 Confinement	7
		2.1.2 The Ghost-Gluon Vertex	S
		2.1.3 Gluon and Ghost Propagator	10
		2.1.4 The Three-Gluon Vertex	12
	2.2	Dyson-Schwinger Equations (DSEs)	13
		2.2.1 Derivation of Dyson-Schwinger Equations	13
		2.2.2 Dyson-Schwinger Equations of Yang-Mills Theory	15
		2.2.3 Skeleton Expansion	15
3	Mat	hematical Prerequisites	19
•	3.1	-	19
	3.1	3.1.1 Pochhammer Symbol	19
		3.1.2 Gaussian Hypergeometric Series of One Variable	21
		3.1.3 Generalized Hypergeometric Series of One Variable	22
		3.1.4 Gaussian Hypergeometric Series of Two Variables	23
		3.1.5 Convergence of Double Hypergeometric Series	24
	3.2	Appell's Series F_4	26
		3.2.1 Definition and Convergence	26
		3.2.2 Analytic Continuation	
	3.3	Negative Dimensions Integration Method	29
4	Resi	ulto	35
4	4.1	Naive Power Counting	
	4.1	9	
	4.0		
	4.2	Calculation of the Ghost Triangle	43
		4.2.1 The Ghost Triangle	43
		4.2.2 Solution to the Massless Three-Point Integral	45
		4.2.3 Euclidean Region	
		4.2.4 Tensor Components	50

Contents

5	Conclusions	53
Α	Conventions, Notations and FormulasA.1 PropagatorsA.2 VerticesA.3 Gamma Function and Pochhammer Symbol	58
В	Analytic Continuation of Appell's Function F_4 into the Euclidean Momentum Region	65

1 Introduction

In popular physics books one often finds the statement that the basic physical theories, which describe our universe, are known. These are the theories of gravitation, of the electroweak and of the strong interaction. This might give a wrong impression, since it is true that this theories are known, but for example quantum chromodynamics (QCD), the theory of the strong force and subject of this thesis, is far from being solved. Indeed, this theory is older than 30 years, but it still puzzles physicists. The theory of the electromagnetic interaction, quantum electrodynamics (QED), is quite well understood. Like QCD it is a gauge theory. The difference lies in the non-Abelian nature of QCD, which does not only allow interaction between quarks and gluons, the elementary particles of it, but also among gluons themselves. This complicates the theory enough to occupy physicists for decades now.

To understand QCD lots of frameworks have been devised, which work more or less well. A successful approach is perturbation theory which can only access the high energy region of QCD. At lower energies, i.e. large distances, phenomena like confinement and chiral symmetry breaking occur. For these scales perturbation theory is not valid, because it employs an expansion in the coupling, which is not possible here as the strength of the interaction becomes too large. Therefore a need arises for other possibilities to describe the phenomenology of QCD such as confinement, which means the fact that nature does not allow single quarks or gluons in physical states. They are only observed in objects called hadrons, which have the property to be colorless in contrast to quarks and gluons. In fact the name quantum chromodynamics derives from attributing the fictitious property of color to quarks and gluons.

Another method are Monte-Carlo simulations on a discretized space-time. They suffer from limitations due to finite size effects, but they provide an important possibility for comparison, because they include all non-perturbative effects of Yang-Mills theory, which can be extracted in the infinite volume limit. A complementary approach are Dyson-Schwinger equations (DSEs), which are used in this thesis. They have the advantage to be valid for all energies. Unfortunately their structure is very intricate. Nevertheless they have become an indispensable tool during the last decade.

Confinement has long been known to be a basic property of QCD. However, a satisfying explanation is still lacking. Current efforts try to describe confinement for pure gluodynamics, or also known as Yang-Mills sector of QCD. Thereby the quarks are considered

static and only the dynamics of the gluons is investigated. Depending on the chosen gauge also another type of particles occurs, called ghosts. These are no physical particles in the proper sense: They appear in calculations but never in results for observable quantities. Including quarks is the next step to complete the picture of confinement. Before doing that verifications of the scenario for the Yang-Mills sector are indispensable, i.e. different approaches like DSEs, renormalization group or Monte-Carlo simulations should be compared.

Neglecting quarks simplifies the calculations with Dyson-Schwinger equations and starting from the solutions for the propagators of ghosts and gluons [1] further investigations were made in the infrared region, i.e. at low momenta below a few hundred MeV. The systematic treatment of vertex functions was pioneered by Alkofer, Fischer and Llanes-Estrada [2], who showed that a power counting procedure is enough to determine the behavior of vertices in the infrared. Their results supported the assumption that the ghosts play a crucial role for the confinement of gluons. However, a comparison to Monte-Carlo simulations is not possible yet: For the propagators this works out comparatively well, not at last because the behavior as predicted by infrared Dyson-Schwinger investigations already starts at a few hundred MeV, but for example for the three-gluon vertex data is still inconclusive. For the time being calculations on the lattice are done in lower dimensions, e.g. [3], and a direct comparison with the results of Alkofer et al. is not possible, since they were calculated in four dimensions.

The main object of this thesis is to check if the qualitative behavior of vertex functions according to [2] is also valid in two and three dimensions. If so, Monte-Carlo simulations for two and three dimensions can provide relevant information about Yang-Mills theory in four dimensions. As the infrared region will first be accessed on such lower dimensional lattices, a comparison to qualitative statements in these dimensions is necessary. In addition to the power counting scheme also a complete analytic calculation of the ghost triangle is done, which is the dominant part in the infrared in the first order of the skeleton expansion of the three-gluon vertex.

The outline of this thesis is as follows: Starting in Chapter 2, I will summarize shortly the basic physics which is necessary for the subsequent chapters. Afterwards mathematical tools such as hypergeometric functions and the Negative Dimensions Integration Method are introduced. The results are presented in Chapter 4, which is divided in two sections: In the first one I derive the infrared exponents of vertex functions in d dimensions via a naive power counting procedure, which is supported by analytic results for the three-gluon vertex in the second section. A detailed derivation of the formula for the three-point integral, which is employed for the analytic calculations, is included there. The last chapter consists of the conclusions. Details on conventions and notations are written down in Appendix A, where also a useful collection of formulas for Gamma functions and Pochhammer symbols can be found. The analytic continuation necessary for the three-point integral in Euclidean space-time is derived in Appendix B.

2 Underlying Physical Concepts

In this chapter I explain the basic physics forming the foundations of this thesis, which are the infrared region of QCD and the Dyson-Schwinger approach to it. Special attention is given to confinement and to the behavior of propagators and vertices at low momenta. In the Dyson-Schwinger part I sketch the derivation of Dyson-Schwinger equations and how they can be simplified via a skeleton expansion.

For conventions and notations see Appendix A.

2.1 The Infrared Region of QCD

The high-energy sector of QCD is accessible via perturbation theory which employs a special property of QCD called asymptotic freedom and allows for an expansion in the coupling. At low momenta, i.e. below a few hundred MeV, this approach does not work any longer and phenomena as confinement and chiral symmetry breaking need other methods to be dealt with.

Such alternative non-perturbative approaches are the exact renormalization group, Dyson-Schwinger equations or lattice Monte-Carlo simulations. The latter discretize the continuum and have the advantage that - at least in principle - all quantum effects of the theory are included. However, due to finite computer power lattices are restricted in size. Thus calculations are only possible for certain regions of momenta and finite size effects occur. One way out are lattices in lower dimensions which have been proven especially useful in the infrared. In regions that are accessible to lattice Monte-Carlo simulations they provide a good possibility for comparison with other methods. In this work the Dyson-Schwinger approach will be employed whose advantages and problems are described in section 2.2.

2.1.1 Confinement

The expression confinement means the fact, that nature does not allow colored particles, i.e. quarks and gluons, to be observed directly. Evidence that particles like protons and neutrons consist of point-like particles is provided by deep inelastic scattering. Confinement is still not understood and has been object of investigations for decades now. Many

believe that the reason for confinement lies in pure gluodynamics, but it was long not clear if one has "confining" or "confined" gluons [4]. The former means an infrared divergent gluon propagator and the latter an infrared finite or even vanishing one. Whereas earlier an infrared slavery scenario, i.e. confining gluons, was favored, there has been a change of mind nowadays and there are many hints for an infrared vanishing gluon propagator. Especially studies of Dyson-Schwinger equations and the renormalization group caused the change in that direction. For more details see refs. [4, 5] and references therein.

One scenario that describes confinement is the so-called Gribov-Zwanziger scenario. Before explaining what it is, I will shortly summarize facts about the Gribov horizon. In the naive definition of the generating functional of a gauge field theory one integrates over all gauge field configurations. Thereby, configurations which describe the same physical states are encountered due to the gauge symmetry of the theory. These states, that are connected via gauge transformations, form a so-called gauge orbit [A]. Thus, the integral should only take into account distinct gauge field configurations, i.e. every gauge orbit should only occur once in the integration process. One can do so with the Faddeev-Popov method (or so one thought) [6, 7, 8] which fixes the gauge via a gauge-fixing condition, e.g. $\partial_{\mu}A_{\mu}=0$ for linear covariant gauges. In the space of field configurations this condition defines a hyperplane. A sketch of configuration space is depicted in fig. 2.1. The gauge-fixing process leads to the appearance of ghosts (in most gauges) via the Faddeev-Popov determinant.

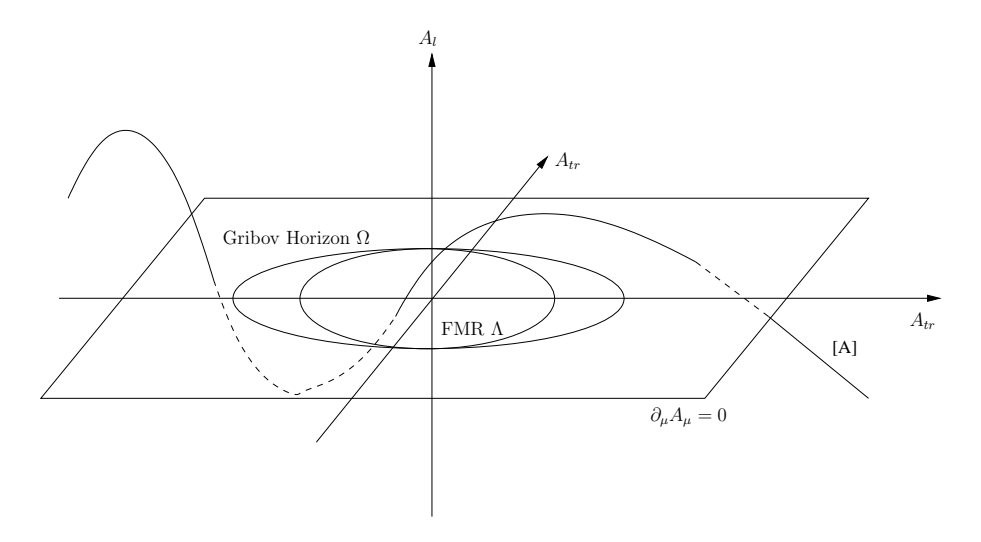


Figure 2.1: A sketch of the space of all gauge configurations. $\partial_{\mu}A_{\mu}=0$ is the gauge condition for linear covariant gauges and defines a hyperplane, Ω is the (first) Gribov horizon and Λ the fundamental modular region (FMR). [A] is a gauge orbit that intersects the total hyperplane several times, but the FMR only once.

Gribov, however, showed in 1978 [9], that this method does not restrict the integration to

only one representative of a gauge orbit and a gauge orbit can intersect the hyperplane defined by the gauge-fixing condition several times. These configurations are called Gribov copies. If one wants to restrict the integration to only one representative per gauge orbit, only the gauge field configurations that lie inside the (first) Gribov horizon, often denoted by Ω , should be considered. The Gribov horizon is defined such, that it contains only those configurations along the gauge orbit that are *locally* minimal with respect to gauge transformations. Unfortunately this does not suffice either, as van Baal explained with *More* (Thoughts on) Gribov Copies [10]. For really having only one single copy of a gauge one needs the fundamental modular region (FMR), which is the region that contains only the global minima of the gauge orbits.

In perturbation theory one has the fortunate situation that one does not really have to care about the Gribov horizon or the FMR, because the origin of the space of gauge field configurations lies within them. And as perturbation theory is an expansion around the origin (and therefore only valid in its "neighborhood") it has no problems with gauge copies.

The Gribov-Zwanziger scenario can be summarized by the following two statements [5]:

- The dressed gluon propagator vanishes in the infrared [11].
- The dressed ghost propagator is more singular in the infrared than a simple pole [12]. This is a consequence of the Gribov horizon.

The idea behind this is that gauge field configurations near the Gribov horizon, or more precisely near the common boundary of the Gribov horizon and the FMR, $\partial\Omega \cap \partial\Lambda$, are responsible for the infrared behavior of Yang-Mills theory.

Another confinement scenario, the Kugo-Ojima scenario [13], has the same property for the ghost propagator and a less strict one for the gluon propagator: There it only has to be less singular than a simple pole.

For more details on the propagators see section 2.1.3.

2.1.2 The Ghost-Gluon Vertex

An important issue is the fact that in Landau gauge the ghost-gluon vertex remains bare for vanishing incoming momentum and stays bare in the ultraviolet due to its non-renormalization [14, 15], i.e. its renormalization constant \tilde{Z}_1 is finite and can even be chosen as one. This justifies the use of a bare vertex instead of a dressed one and simplifies DSEs containing a dressed ghost-gluon vertex immensely. It is used in both numerical solutions of the coupled system of integral equations of gluon and ghost DSEs [1] and in analytic investigations as done in this work. I will shortly outline the idea behind the non-renormalization of the ghost-gluon vertex.

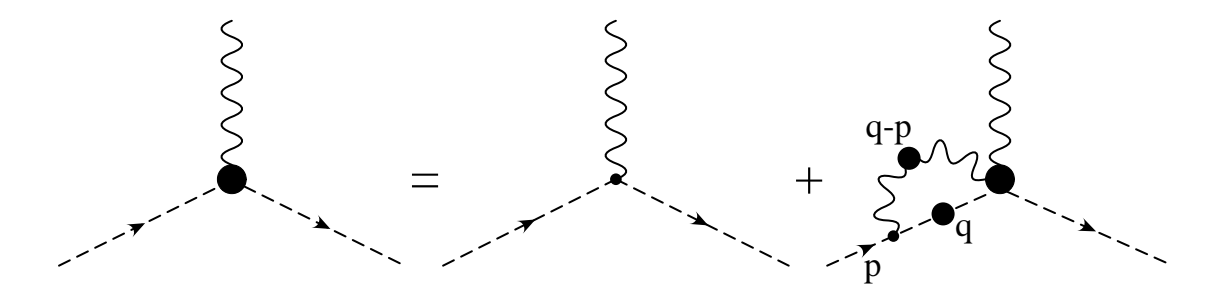


Figure 2.2: The ghost-gluon vertex DSE.

The essential ingredient is the transversality of the gluon propagator in Landau gauge. The transversality can directly be seen from looking at the contraction of the gluon propagator, eq. (A.1), with a momentum vector:

$$k_{\mu}D_{\mu\nu}(k) = k_{\mu}\frac{Z(k)}{k^2} \left[\delta_{\mu\nu} - \frac{k_{\mu}k_{\nu}}{k^2}\right] = 0.$$
 (2.1)

From this follows $(q-p)_{\mu}D_{\mu\nu}(q-p)=0$ and therefore $q_{\mu}D_{\mu\nu}(q-p)=p_{\mu}D_{\mu\nu}(q-p)$. So when the momentum p goes to zero, $q_{\mu}D_{\mu\nu}(q-p)$ vanishes. Now we have a look at the ghost-gluon DSE which is depicted in fig. 2.2. In the second Feynman diagram on the right hand side we have a loop momentum q and an external momentum p. The bare ghost-gluon vertex is proportional to q, as q is its outgoing ghost momentum, and the gluon propagator gives the contribution $D_{\mu\nu}(q-p)$. So we have the expression from above, $q_{\mu}D_{\mu\nu}(q-p)$, which is 0 for vanishing p. As a consequence the whole second diagram vanishes for zero external momentum. If in addition the renormalization constant of the ghost-gluon vertex is defined at $\mu^2=0$,

$$G_{\mu}^{abc}(q,p)|_{k^2=q^2=p^2=0} = \tilde{Z}_1 G_{\mu}^{(bare)abc}(q,p),$$
 (2.2)

the renormalization constant \tilde{Z}_1 is 1.

The bare ghost-gluon vertex is supported also by DSE investigations [16] and lattice simulations [17, 18]. Lattice results exist also for three [3] and two dimensions. With both methods one sees that only in the mid-momentum region there are minor deviations from the bare vertex.

2.1.3 Gluon and Ghost Propagator

As mentioned above there exist two possibilities for the infrared behavior of gluons: infrared enhanced (confining) gluons and infrared finite or vanishing (confined) gluons. The

former were long favored, but nowadays evidence grows that the gluon propagator is indeed vanishing in the infrared. From the viewpoint of DSEs this development might seem better understandable when one compares earlier and recent DSE studies.

When trying to solve the coupled system of equations of the infinite DSE tower one naturally has to resort to truncations and approximations. An early suggestion for calculating the gluon propagator came from Mandelstam [19] who proposed to neglect ghosts. This was justified by small numerical ghost contributions in perturbation theory. The fourgluon vertex was also neglected, which is understandable from the viewpoint of perturbation theory as it only occurs at two-loop order. He furthermore alleviated the calculation by an approximation for the dressed three-gluon vertex such that it compensated together with one gluon dressing function to a bare vertex. What was left is the DSE depicted in fig. 2.3 which only contains bare quantities and the dressed gluon propagator. Mandelstam himself recognized that a solution to this equation required the gluon propagator to be divergent for vanishing momenta. The Mandelstam approximation was investigated subsequently for example by Brown and Pennington [20], who also reasoned for negligible ghosts with the small numerical contributions of the ghost loop at one-loop order in perturbation theory. They even referred to another work [21], where the bare ghost propagator had been taken into account but only small differences had occured. A more recent calculation can be found in [22] which affirmed the earlier results: The Mandelstam approximation yields a divergent gluon in the infrared and also the running coupling is singular for low momenta.

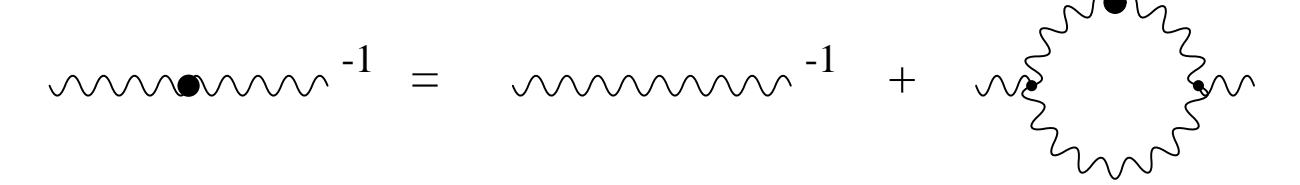


Figure 2.3: The gluon DSE in the Mandelstam approximation.

The situation changed with the work by von Smekal, Hauck and Alkofer [1]. They solved the coupled DSEs for gluon and ghost propagator in Landau gauge. Of course, they also had to make approximations, namely neglect four-point correlation functions (four-gluon vertex function and irreducible scattering kernels). The three-point vertex functions, however, were taken into account by constructing them from their Slavnov-Taylor identities which impose certain restrictions on the vertices but do not fully constrain them. The result showed a completely different behavior than previous ones: The ghosts turned out to give the dominant contribution in the infrared, whereas the gluon propagator vanished. The running coupling, singular in the Mandelstam approximation, had now an infrared fixed point.

The evidence for this new picture is growing and further investigations were done as well

in the DSE approach, for instance in [23], as with other methods (stochastic quantization, functional renormalization group). Also data from lattice Monte-Carlo simulations exists which indicates a divergent ghost propagator, e.g. in [3, 24]. The gluon propagator, however, shows a behavior that is different from the continuum, namely it seems to be finite which contradicts the Gribov-Zwanziger scenario. Of course, this could be lattice artifacts and bigger lattices should approach the continuum limit. This issue was addressed in [25, 26] where DSEs were calculated on a compact manifold. The results showed good agreement with lattice data, but the infinite volume limit was approached very slowly so that one cannot expect lattice Monte-Carlo simulations to yield directly the correct results in the near future.

To describe the behavior of ghost and gluon propagators in the infrared in the present picture one needs only one constant, usually denoted by κ . The infrared exponents of the propagators, which determine the momentum dependence of the dressing functions at low momenta, both depend only on this constant κ . The ghost and gluon dressing functions G and Z are expected to behave as

$$G(p^2) \propto (p^2)^{-\kappa}$$
 $Z(p^2) \propto (p^2)^{2\kappa}$ (2.3)

in the infrared. This result will be derived in section 4.1.2 for arbitrary dimension d. The value of κ depends on the number of dimensions. In four dimensions we have [27, 28]

$$\kappa = \frac{93 - \sqrt{1201}}{98} \approx 0.595. \tag{2.4}$$

The value for other dimensions can be found in [29, 28]. For two and three dimensions there exist two possible solutions each: approximately 0.4 and exact 0.5 in three and 0.2 and 0 in two dimensions. Which are correct still has to be determined.

2.1.4 The Three-Gluon Vertex

The next step after solving the DSEs for the propagators is concerned with the vertices of Yang-Mills theory (except the ghost-gluon vertex, see section 2.1.2). The first who treated the infrared behavior of all vertices systematically in a DSE approach were Alkofer, Fischer and Llanes-Estrada in [2] where they calculated the infrared exponents of arbitrary Green functions. An outline of their approach is given in section 4.1.1. They showed that the three-gluon vertex diverges as $(p^2)^{-3\kappa}$. For arbitrary n-point functions with n ghost-antighost-pairs and m gluons they found the momentum dependence to be $(p^2)^{(n-m)\kappa}$, so that all Green functions can be described by the same κ and the inclusion of vertices does not lead to an additional constant. Unfortunately calculations for the three-gluon vertex are hardly feasible on the lattice in four dimensions, but there exists data in two and three [3]. A comparison between three and four dimensions can be found in [18]. The data raises

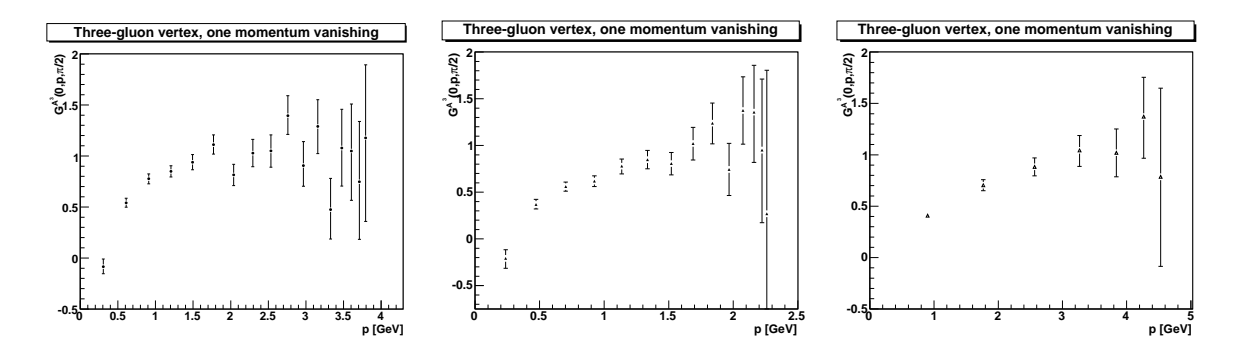


Figure 2.4: Lattice results for the three-gluon vertex in two [30], three [3] and four dimensions [18]. Clearly the situation is better in two and three dimensions.

new questions, as the three-gluon vertex does not seem to diverge for zero momentum, see fig. 2.4. The fact, however, that the calculated tensor component changes sign indicates that we do not see the infrared behavior of the three-gluon vertex, as the expected scaling behavior does not allow a change of sign. This is in contrast to ghosts and gluons, where one can see the infrared scaling behavior already at a few hundred MeV.

2.2 Dyson-Schwinger Equations (DSEs)

Dyson-Schwinger equations - or sometimes called Schwinger-Dyson equations - are named after F. J. Dyson [31] and J. S. Schwinger [32, 33] who were the first to derive them in 1949 and 1951 respectively. A DSE is the equation of motion of a Green function in form of an integral equation. DSEs can be derived for every Green function in a field theory, but unfortunately one DSE cannot stand alone because it is embedded into a stack of infinitely many DSEs. The reason for this is that every DSE for an n-point function contains higher n-point functions and a closed system is thus not possible. So when trying to solve a DSE the tricky part are the necessary truncations and approximations. How involved the choice of a suitable approximation is one can see for example when considering the Mandelstam approximation, which was shortly outlined in section 2.1.3. The results from this approximation (neglecting ghosts) were contradicted by later investigations which also took into account ghosts. This is only one example that the validity of a truncation needs to be verified.

2.2.1 Derivation of Dyson-Schwinger Equations

The derivation of DSEs is not described in many books. As a matter of fact the only books known to me that treat DSEs are the books of Itzykson and Zuber [34] and Rivers

[35]. In the papers by Alkofer and von Smekal [4] and Roberts and Williams [36] one can find details about the DSEs of QED and QCD. Derivations of some DSEs can be found in the following references:

• photon: p. 476ff. in [4], [34]

• electron: p. 477ff. in [34]

• quark: [4]

• ghost propagator: [4]

• ghost-gluon vertex: [16]

The papers of Eichten and Feinberg [37] and Baker and Lee [38] can also provide additional information on the derivations.

In general there exist two possible ways to derive a DSE. One is described in [35] and uses Heisenberg's equation of motion and the equal time commutation relations. The second one is more common and employs the fact that the integral of a total derivative vanishes. I will only give a short description of how the second method works. Starting point is the generating functional $Z[J, \bar{\sigma}, \sigma]$ of the full Green functions, where $J, \bar{\sigma}$ and σ are gluon, ghost and anti-ghost sources (the normalization factor is omitted):

$$Z[J,\bar{\sigma},\sigma] = \int D[A\,c\,\bar{c}] \exp(-S_{YM} + \int d^d x (A\,J + c\,\bar{\sigma} + \bar{c}\,\sigma)). \tag{2.5}$$

When differentiating with respect to a field ϕ , which can be a gluon (A), a ghost (c) or an anti-ghost (\bar{c}) field, the integral vanishes:

$$0 = \int D[A c \,\bar{c}] \left(-\frac{\delta S_{YM}}{\delta \phi} + j\right) \exp\left(-S_{YM} + \int d^d x (A J + c \,\bar{\sigma} + \bar{c} \,\sigma)\right). \tag{2.6}$$

Here j denotes the corresponding source to ϕ . To get the DSE for an n-point function one has to make further derivatives and to set the sources to zero afterwards. For the DSEs of connected or one-particle irreducible Green functions one can apply the same procedure to the generating functionals of them, which are defined as

$$W[J, \bar{\sigma}, \sigma] = \ln(Z[J, \bar{\sigma}, \sigma]) \tag{2.7}$$

and

$$\Gamma[A, c, \bar{c}] = -W[J, \bar{\sigma}, \sigma] + \phi j \tag{2.8}$$

respectively. Γ is also known as effective action. The derivation above is quite formal and real calculations prove to be quite tedious.

2.2.2 Dyson-Schwinger Equations of Yang-Mills Theory

Without quarks we have the following primitively divergent n-point functions in Yang Mills theory: gluon and ghost propagator, ghost-gluon, three-gluon and four-gluon vertex. As an example of what a DSE looks like we consider the easiest DSE of QCD, the DSE for the ghost propagator which is depicted in fig. 2.5.

Its graphical representation allows an intuitive interpretation: The left hand side includes all possibilities for a ghost to propagate. The first diagram on the right hand side shows a ghost that propagates without any interaction, which can of course happen. But in the second diagram we see what he can do alternatively on his way, namely he can split up into another ghost and a gluon in the bare ghost-gluon vertex. These two new particles propagate themselves in all possible ways, therefore the dressed propagators. At the end they have to join again, but of course also in all possible ways, hence the dressed vertex. The additional dressed quantities lead to the infinite tower of integral equations, because they have their own DSEs. The bare and proper propagators occur in inverse form here, because they are also inverse in the Lagrangian and in the effective action Γ .



Figure 2.5: The DSE for the ghost propagator.

The structure of the DSE for the ghost propagator seems rather simple. The reason is that a ghost does not have so many possibilities to interact, namely only one via a ghost-gluon vertex. The gluon on the other hand has additional possibilities because of its self-interaction and its DSE contains four more terms. The ghost-gluon vertex DSE appeared already in section 2.1.2, fig. 2.2. The three-gluon vertex DSE is depicted in fig. 2.6 in section 2.2.3, where a part of its skeleton expansion is treated. From now on all internal propagators are drawn without the full blob but are considered dressed nonetheless, so that the figures get not too overloaded.

2.2.3 Skeleton Expansion

A simple statement what the skeleton expansion is can be found in [5]: a loop expansion using dressed propagators and vertices. Although this might tell the advanced reader everything he or she needs, I will try to give a more detailed description of it in the following.

The skeleton expansion decomposes a diagram of a DSE into several diagrams containing only primitively divergent dressed vertices, i.e. ghost-gluon, three-gluon and four-gluon

vertices, and dressed propagators, whereas the order of the expansion is determined by the number of loops added in this procedure. The basic idea what a skeleton is can be found in [39] on which the following outline is based.

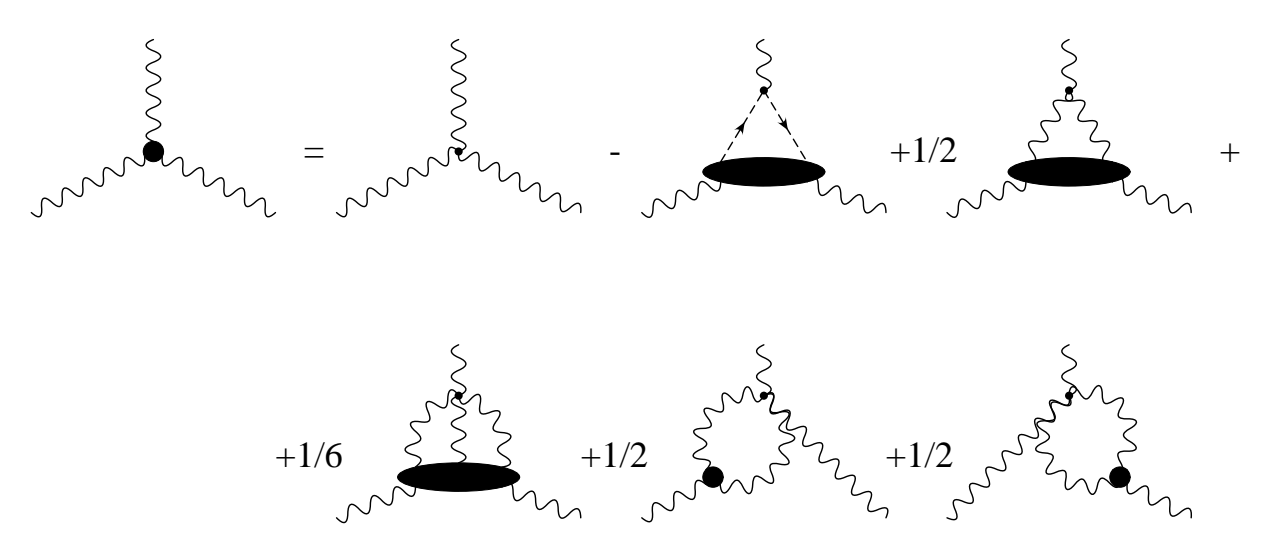


Figure 2.6: The DSE for three-gluon vertex.

At first we have to distinguish between three different sorts of n-point functions: We have the full n-point functions that contain all possible graphs, even not connected ones, connected n-point functions, that as their name already says only have contributions from connected diagrams, and proper or one-particle-irreducible n-point functions, which contain only connected graphs that cannot be separated into two by cutting one internal propagator line. Every n-point function gets contributions from all possible combinations of propagators and vertices that do not violate its intrinsic properties, i.e. a connected diagram still has to be connected. The expression skeleton now refers to a graph in which all propagators and vertices are bare. By adding the "flesh", that means inserting full, connected or proper n-points functions instead of the bare ones, one can reconstruct all graphs that lead to this skeleton graph. In this sense skeleton graphs are unique for each diagram.

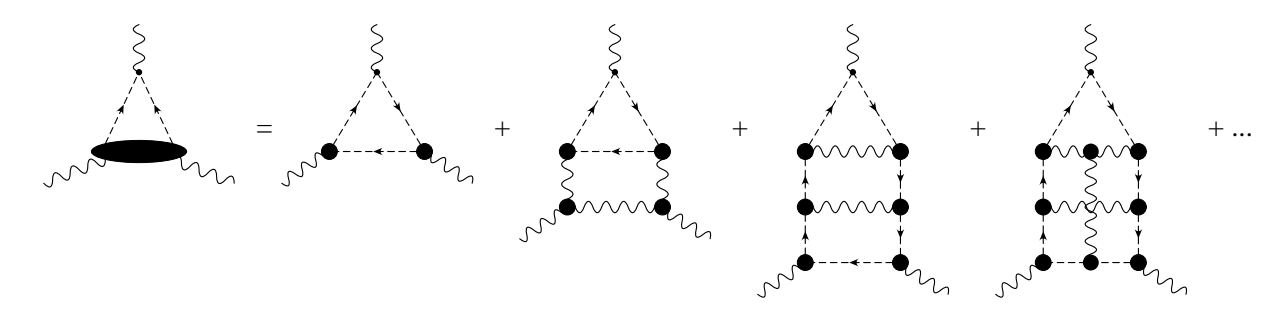


Figure 2.7: Skeleton expansion of the ghost triangle.

What do we need this for? Consider for example the DSE for the three-gluon vertex, fig. 2.6, which contains the two-ghost-two-gluon scattering kernel in the third diagram. The problem of this diagram is that we do not know what to do with the scattering kernel as its own DSE contains even higher n-point functions. A possible way is to consider all distinct diagrams that contribute to it. A few of these diagrams are depicted in fig. 2.7. The good thing about this expansion is, that higher orders do not have a different infrared exponent as will be demonstrated in section 4.1.2. At the same time this is the problem of the skeleton expansion: One does not know how much each single diagram contributes but all diagrams contribute with the same infrared exponent and there are no infrared suppressed ones.

To construct the skeleton expansion of a diagram one can use the insertions given in fig. 2.8. Starting from the simplest diagram that is possible to construct with primitively divergent n-point functions one inserts these additional dressed vertex functions and propagators. Thereby the number of loops increases. The complete skeleton expansion of the three-gluon vertex DSE in first order can be found in fig. 4.3.

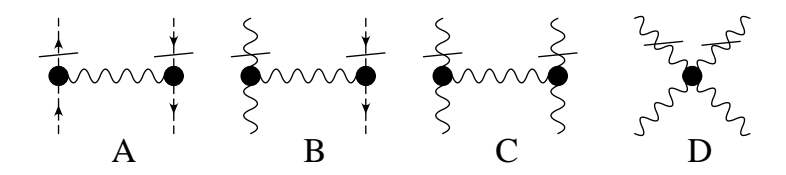


Figure 2.8: Insertions that lead to higher orders in the skeleton expansion.

3 Mathematical Prerequisites

In the analytic calculation of the ghost triangle an approach for the integral called Negative Dimensions Integration Method (NDIM) will be used. Therefore I give a brief overview of NDIM in the third section of this chapter. As the results of NDIM in the general case turn out to consist of (Gaussian) hypergeometric series, an introduction to them can be found in the first section. In the case of the massless three-point integral we need Appell's series F_4 which is explained in some more detail in the second section. Although much is known about this series the direct result obtained with NDIM is not usable when calculating with Euclidean metric, because it does not converge in the Euclidean momentum region. The way out is also explained in the section about Appell's series F_4 .

3.1 Hypergeometric Series

3.1.1 Pochhammer Symbol

When dealing with hypergeometric series some knowledge about the Pochhammer symbol is necessary. The Pochhammer symbol is named after L. A. Pochhammer (1841-1920). It is especially useful when handling hypergeometric series. For the reader, who is not familiar with it, I summarize a few important relations which are used in this work. The most extensive summary about the Pochhammer symbol I found in [40], but its definition can also be found for example in [41].

Various notations are used:

$$(a,m) \equiv (a)_m \equiv (a|m). \tag{3.1}$$

I will stick to the first one. Sometimes the Pochhammer symbol is also referred to as the factorial function, since (1, n) = n!. The initial definition for integer values of the second argument is

$$(a,n) = \begin{cases} 1 & n=0 \\ a(a+1)\dots(a+n-1) & n=1,2,3,\dots \end{cases}$$
 (3.2)

This can also be expressed in terms of gamma functions, whereby a generalization to non-integer values is possible:

$$(a,n) = \frac{\Gamma(a+n)}{\Gamma(a)}. (3.3)$$

Simply by applying the above definition, one can show the validity of the next equation:

$$(a, m+n) = (a, m)(a+m, n). (3.4)$$

Now I will proof an important formula for the Pochhammer symbol, the formula for the analytic continuation. Consider the binomial coefficient, given for real a and non-negative integer n by

$$\binom{a}{n} = \frac{a(a-1)\dots(a-n+1)}{n!}.$$
(3.5)

With the above definition for the Pochhammer symbol, eq. (3.2), we can write this as

$$\binom{a}{n} = \frac{(-1)^n (-a, n)}{n!} \tag{3.6}$$

or with gamma functions as

$$\binom{a}{n} = \frac{\Gamma(a+1)}{n!\Gamma(a-n+1)}.$$
(3.7)

Therefore we have with a = b - 1

$$\frac{\Gamma(b)}{n!\Gamma(b-n)} = \frac{(-1)^n (1-b,n)}{n!}.$$
(3.8)

This we can use as a definition for the Pochhammer symbol, when the second argument is negative:

$$(a, -n) = \frac{(-1)^{-n}}{(1 - a, n)}. (3.9)$$

So we expanded the original definition to all integer values of n. In principle the Pochhammer symbol can also be given for non-integer values n by eq. (3.3), but the formula for the analytic continuation, eq. (3.9), is then no longer valid (as can be directly seen by considering $(-1)^n$). However, with an integer n eq. (3.9) will prove quite useful.

With Legendre's duplication formula,

$$\Gamma(2a) = \frac{\Gamma(a)\Gamma(a+1/2)}{2^{1-2a}\sqrt{\pi}},$$
(3.10)

one can derive an equivalent equation for the Pochhammer symbol:

$$(a, 2b) = 2^{2b}(a/2, b)(1/2 + a/2, b). (3.11)$$

Using NDIM one often ends up with gamma functions that have to be transformed into

Pochhammer symbols. This is easily achieved by using

$$\Gamma(a+n) = \Gamma(a)(a,n). \tag{3.12}$$

For convenience one can derive a set of such transformation formulas which turn out to be quite useful when using NDIM. In Appendix A one finds a list of important equations for Pochhammer symbols and Gamma functions.

3.1.2 Gaussian Hypergeometric Series of One Variable

The definition of the Gaussian hypergeometric series is [41] (\mathbb{Z}_0^- is defined as the set of non-positive integer numbers)

$$F(a,b;c;z) = \sum_{n=0}^{\infty} \frac{(a,n)(b,n)}{(c,n)} \frac{z^n}{n!}, \quad c \notin \mathbb{Z}_0^-.$$
 (3.13)

It can be regarded as a generalization of the geometric series

$$\sum_{n=0}^{\infty} z^n = 1 + z + z^2 + \dots; (3.14)$$

thus the name *hypergeometric* series. It was introduced 1812 by C. F. Gauss (1777-1855) and is named after him Gaussian hypergeometric series. He also introduced the F-notation for it. A good overview of (Gaussian) hypergeometric series can be found for example in [40].

The use of the expression hypergeometric deserves some caution. Sometimes, especially in [40], the term hypergeometric series is used in the sense of Gaussian hypergeometric series. In general the expression hypergeometric series is used in a wider sense, denoting series whose coefficients are rational functions of the summation index/indices, see section 3.1.5. A further comment on labeling expressions: When talking about parameters, the expressions in the Pochhammer symbols are meant, e.g. a, b or c in eq. (3.13), whereas variables refer to the expression(s) which are exponentiated, e.g. x in eq. (3.13).

Applying d'Alembert's ratio test [42] yields an absolute convergence within the unit circle, |z| < 1. When |z| = 1 the convergence depends on the parameters [41]:

- Absolutely convergent if Re(c-a-b) > 0.
- Conditionally convergent if $-1 < Re(c-a-b) \le 0, z \ne 1$.
- Divergent if $Re(c-a-b) \leq -1$.

Note two cases of special parameters:

- $c = m \in \mathbb{Z}_0^-$: The series is undefined, except a or $b = n \in \mathbb{Z}_0^-$ with n > m.
- a, b or both $\in \mathbb{Z}_0^-$: The hypergeometric series terminates and there is no question of convergence because for a finite argument we have a finite result.

More on the Gaussian hypergeometric series one can find in [41] in Chapter 15 or in [43], p. 412-417 and p. 430-434.

3.1.3 Generalized Hypergeometric Series of One Variable

Introducing an arbitrary number of parameters, one can define a generalized hypergeometric series [40]:

$${}_{p}F_{q}(a_{1},\ldots,a_{p};b_{1},\ldots,b_{q};z) \equiv$$

$$\equiv {}_{p}F_{q}\begin{pmatrix} a_{1},\ldots,a_{p};\\b_{1},\ldots,b_{q}; \end{pmatrix} = \sum_{n=0}^{\infty} \frac{(a_{1},n)\ldots(a_{p},n)}{(b_{1},n)\ldots(b_{q},n)} \frac{z^{n}}{n!}, \qquad p,q \in \mathbb{N}_{0}.$$
(3.15)

With generalized hypergeometric series one can express many functions. Just to provide an impression I give here three elementary examples [40], where * stands for zero arguments:

$$e^z = {}_0F_0(*; *; z),$$
 (3.16)

$$ln(1+z) = z {}_{2}F_{1}(1,1;2;-z),$$
(3.17)

$$\cos z = {}_{0}F_{1}(*; \frac{1}{2}; -\frac{1}{4}z^{2}). \tag{3.18}$$

The original Gaussian hypergeometric series F can now be written as ${}_{2}F_{1}$. In general we can make the following statements about convergence of these generalized hypergeometric series [40]:

- Convergence for $|z| < \infty$ if $p \le q$.
- Convergence for |z| < 1 if p = q + 1.
- Divergence for all $z \neq 0$, if p > q + 1.

This is valid except for the cases when

- one of the parameters in the denominator, $b_i = m$, is 0 or a negative integer: The series is divergent. Exception: One of the parameters in the numerator, a_i , is $n \in \mathbb{Z}_0^-$ with n > m.
- one of the parameters in the numerator, a_i , is 0 or a negative integer: The series terminates and we have a finite result.

More material about generalized hypergeometric series one can find in [43], p417-426, p. 437-448 and p. 453-615.

3.1.4 Gaussian Hypergeometric Series of Two Variables

A generalization from one to two and more variables is possible. A multiple Gaussian hypergeometric series is then defined to be a series of several variables which reduces to the Gaussian hypergeometric series in one variable when only one variable is non-zero. This definition limits the number of possible series that are Gaussian hypergeometric series: For two variables there exist 14 series, for three 205 [40]. Another form of series are confluent series, which I mention here for completeness. They reduce to the generalized hypergeometric series ${}_2F_1$, ${}_1F_1$ or ${}_0F_1$ when only one variable is non-zero, but not in all cases to ${}_2F_1$ [40].

The double Gaussian hypergeometric series were found in two steps: The first four were written down by P. Appell (1855-1930) in 1880 in [44] and named after him Appell's series F_1 , F_2 , F_3 and F_4 . F_4 will become important in calculating the ghost triangle of the three-gluon vertex in section 4.2. The remaining ten Gaussian hypergeometric series are known as Horn series after J. Horn who defined in 1931 G_1 , G_2 , G_3 , H_1 , H_2 , H_3 , H_4 , H_5 , H_6 and H_7 in [45]. This should not give the impression that these 14 functions were only known since 1880 and 1931 respectively, but Appell and Horn were the first to make some systematic studies. A common property of the double Gaussian and confluent hypergeometric series is, that they are the 34 double hypergeometric series of order two. The order of a hypergeometric series is only a descriptive term [40] and its definition can be found below in section 3.1.5.

As $_pF_q$ is a generalization of the Gaussian hypergeometric series with one variable, there exist also generalizations of double Gaussian hypergeometric series. For example Kampé de Fériet generalized the four Appell series to an arbitrary number of parameters in the numerator and denominator [46]. There exist also Gaussian hypergeometric series for three or more variables, e.g. the Lauricella series, which are generalizations of the Appell's series to more than two variables [47]. Sometimes one refers to the number of variables as dimension.

Applications of multiple Gaussian hypergeometric series are abundant. Just to give an impression, I quote the following examples: Perturbation theory, Schrödinger equation, heat conduction, mechanics of deformable media, Lie algebras and Lie groups, statistical distributions, genetics; for a more exhaustive list see [40].

3.1.5 Convergence of Double Hypergeometric Series

The determination of the region of convergence for double hypergeometric series is not as easy as for hypergeometric series in one variable (d'Alembert's ratio test). What we need, is the theorem of Horn on the convergence of double hypergeometric series.

Generally speaking about the region of convergence makes only sense for values of the parameters for which the series is not undefined, does not terminate (then we always have a finite result for finite arguments) and does not reduce to a sum of hypergeometric series of lower dimension. Appell's series F_2 is defined as

$$F_2(a,b,c;d,e,f;x,y) = \sum_{m,n=0}^{\infty} \frac{(a,m+n)(b,m)(c,n)}{(e,m)(f,n)} \frac{x^m}{m!} \frac{y^n}{n!}.$$
 (3.19)

Examples for such cases, where there is no need to discuss convergence, for it are:

- $a \in \mathbb{Z}_0^-$: The series in m and n terminate.
- b or $c \in \mathbb{Z}_0^-$: The series in m or n respectively terminates and we get the one-dimensional Gaussian hypergeometric function F.
- e or $f = j \in \mathbb{Z}_0^-$: The series is not defined, except a, b or $c = i \in \mathbb{Z}_0^-$ and i > j.

A very useful property is the fact, that the region of convergence for a hypergeometric series does not depend on the parameters, if one excludes the exceptional parameters. A proof of this can be found in [40]. As the region of convergence is independent of the parameters, we can omit them below. In the following I will outline Horn's theorem as it can be found in [40, 48, 49]. The original work is reference [50].

Let us assume we have a double power series

$$F(x,y) = \sum_{m,n=0}^{\infty} C(m,n) x^m y^n.$$
 (3.20)

We define now the two quotients

$$f(m,n) = \frac{C(m+1,n)}{C(m,n)},$$
(3.21)

$$g(m,n) = \frac{C(m,n+1)}{C(m,n)}. (3.22)$$

F is called a hypergeometric series, if f and g are rational functions of m and n, i.e. we can write them as

$$f(m,n) = \frac{F(m,n)}{F'(m,n)},$$
(3.23)

$$g(m,n) = \frac{G(m,n)}{G'(m,n)},$$
 (3.24)

where F, F', G and G' are polynomials in m and n. This expressions also allows the definition of the *order* of a hypergeometric series as the number of the largest degree of F, F', G or G'. From f and g we define

$$\rho(m,n) = \left| \lim_{t \to \infty} f(mt, nt) \right|^{-1}, \tag{3.25}$$

$$\sigma(m,n) = \left| \lim_{t \to \infty} g(m t, n t) \right|^{-1}, \tag{3.26}$$

$$R = \rho(1,0), \tag{3.27}$$

$$S = \sigma(0, 1). \tag{3.28}$$

Now we can derive the region of convergence of an arbitrary double hypergeometric series with variables x and y. Let us start with considering only one sum and neglecting the second one. That means we keep one summation index at zero and consequently only have to deal with a single sum. With d'Alembert's ratio test we can calculate its region of convergence. Doing this we see, that we get R and S respectively. Thereby we have found the maximum values of the so-called associated radii of convergence r and s of s and s are the parametric representation of the curve s which divides the rectangle in two parts. Horn showed that

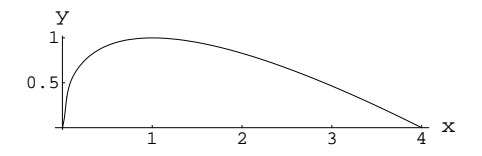
$$r = \rho(m, n), \tag{3.29}$$

$$s = \sigma(m, n). \tag{3.30}$$

The region of convergence is the part of the rectangle where x < r and y < s for all m and n plus the projection of this part onto the coordinate axes. As an example consider the G series that is defined in Appendix B, eq. (B.4). For it we have R = 4, S = 1, $r = \frac{(2\mu + \nu)^2}{(\mu + \nu)^2}$ and $s = \frac{\nu(2\mu + \nu)}{(\mu + \nu)^2}$. This curve is depicted on the left in fig. 3.1. For the complete region of convergence we have to add the part that lies between the curve and the y-axis, see the right picture in fig. 3.1.

The calculation up to now can be done quite easily by hand or even be automated with MATHEMATICA. The tricky part comes now: What we want is an inequality that represents the region of convergence. Therefore one has to build one from the parametric representation of C.

Another method for determining the region of convergence of a hypergeometric function



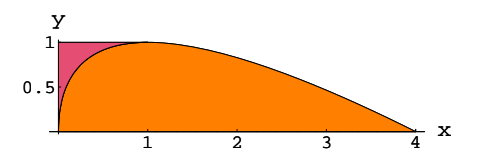


Figure 3.1: The left picture shows the curve defined by r and s for the G series. On the right the complete region of convergence is shown, consisting of the region where x < r and y < s and the part between it and the coordinate axes.

exists. Thereby one makes use of the fact, that the region of convergence does not depend on the parameters. So one can formally choose parameters in such a way, that some Pochhammer symbols cancel each other. This clearly does not work always, but it can shorten calculations. As an example for this technique confer the calculation of the region of convergence of the K series in Appendix B.

3.2 Appell's Series F_4

Appell's series F_4 enters in the calculation of a scalar three-point one-loop diagram without masses. As the ghost triangle is such a diagram and is explicitly calculated in section 4.2, this part treats the definition of Appell's series F_4 , its region of convergence and - very important as will be seen soon - its analytic continuation.

3.2.1 Definition and Convergence

The definition of Appell's series F_4 is

$$F_4(a,b;c,d;x,y) = \sum_{m,n=0}^{\infty} \frac{(a,m+n)(b,m+n)}{(c,m)(d,n)} \frac{x^m}{m!} \frac{y^n}{n!}.$$
 (3.31)

From eq. (3.31) it can be seen that F_4 is symmetric in the parameters a and b. It is not symmetric in c and d. Only a simultaneous exchange of c and d together with x and y yields the original form again.

 F_4 is convergent for

$$\sqrt{|x|} + \sqrt{|y|} < 1. \tag{3.32}$$

This follows from Horns's theorem in section 3.1.5. We can calculate $\rho = \frac{m^2}{(m+n)^2}$, $\sigma = \frac{n^2}{(m+n)^2}$, R = 1 and S = 1. From r and s one gets the inequality above. Unfortunately it will turn out that this condition cannot be fulfilled by the result for the ghost

triangle in Euclidean space-time and an analytic continuation to other values of x and y is necessary.

In our considerations of convergence we have to exclude the following exceptional parameters:

- a or $b \in \mathbb{Z}_0^-$: The series in m and n terminates.
- c or $d = j \in \mathbb{Z}_0^-$: The series is not defined, except a or $b = i \in \mathbb{Z}_0^-$ with i > j.

3.2.2 Analytic Continuation

Although the original Appell's series F_4 is only convergent for $\sqrt{|x|} + \sqrt{|y|} < 1$ analytic continuation makes it possible to consider other regions of the variables. The basic idea behind such a continuation is that there exists a more general quantity that coincides with the series itself in its region of convergence. In the case of Appell's series F_4 this is called Appell's function F_4 . The difference is that the series is only defined for certain values of the variables, but the function is more general and also defined for other values. From complex analysis we know that a meromorphic function has series representations that cover the whole complex plane except at the poles. The respective regions of convergence can thereby only extend until the boundary reaches a pole. In a space with two complex variables this is similar. There are, however, a few differences, see e.g. [51].

One method of getting results for Appell's function F_4 outside the region determined by eq. (3.32) would be transformations of the system of partial differential equations, which Appell's function F_4 fulfills, and of its integral solutions. According to Exton in [49], F_4 is the most intractable of Appell's function, and as a consequence many investigations of the other Appell functions in this approach have been done but hardly of F_4 . Therefore a more straightforwarded method is applied in [49], which I will follow here. It directly transforms the series representation and is more intuitive, but it can be quite tedious.

I will describe now the basic idea of analytic continuation by means of the simplest example existing for F_4 , which extends the series beyond the pole at (0,1); other poles of Appell's function F_4 are at (1,0) and (∞,∞) . This procedure will change the parameters x and y to x/y and 1/y. The result can be found e. g. in [48, 52], where there is a misprint at least in some editions in the exponent of the second (-1): A minus sign is missing there. The correct version can be found in [40, 49, 53]. The first step is to rewrite Appell's series F_4 using eq. (3.4) in such a way, that it contains the Gaussian hypergeometric series in one variable:

$$F_4(a,b;c,d;x,y) = \sum_{m=0}^{\infty} \frac{(a,m)(b,m)}{(c,m)} \frac{x^m}{m!} {}_2F_1(a+m,b+m;d;y).$$
(3.33)

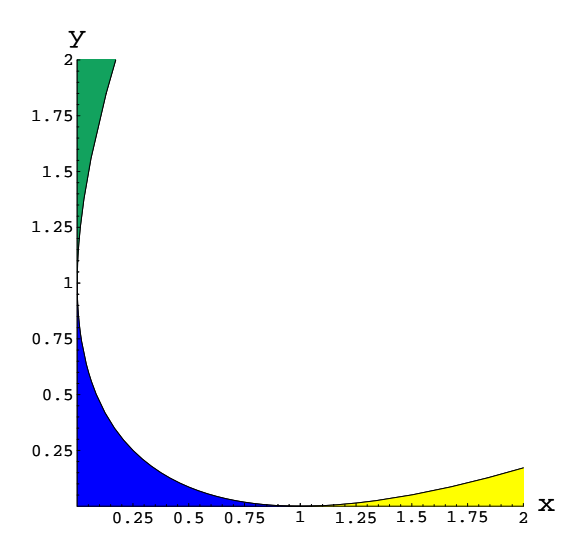


Figure 3.2: Regions of convergence for eqs. (3.31) (blue), (3.35) (green) and (3.37) (yellow).

Now one replaces the Gaussian hypergeometric function ${}_{2}F_{1}$ by its analytic continuation,

$${}_{2}F_{1}(a,b;c;y) = \frac{\Gamma(c)\Gamma(b-a)}{\Gamma(b)\Gamma(c-a)}(-y)^{-a} {}_{2}F_{1}(a,a-c+1;a-b+1;1/y) + \frac{\Gamma(c)\Gamma(a-b)}{\Gamma(a)\Gamma(c-b)}(-y)^{-b} {}_{2}F_{1}(b,b-c+1;b-a+1;1/y),$$
(3.34)

which can be found for instance in [41, 43], and rewrites everything into a form that contains Appell's series F_4 again:

$$F_4(a,b;c,d;x,y) = \frac{\Gamma(d)\Gamma(b-a)}{\Gamma(d-a)\Gamma(b)} (-y)^{-a} F_4(a,a-d+1;c,a+1-b;x/y,1/y) + \frac{\Gamma(d)\Gamma(a-b)}{\Gamma(d-b)\Gamma(a)} (-y)^{-b} F_4(b,b-d+1;c,b+1-a;x/y,1/y).$$
(3.35)

What have we obtained by this? From eq. (3.32) we know, where F_4 is convergent; now, however, the variables have changed from x and y to x/y and 1/y and the region of convergence becomes

$$\sqrt{|x/y|} + \sqrt{|1/y|} < 1. \tag{3.36}$$

We can plot the two regions for comparison, see fig. 3.2, where a third region was added,

derived via the same procedure as above, but with reversed roles of x, m and y, n:

$$F_4(a,b;c,d;x,y) = \frac{\Gamma(c)\Gamma(b-a)}{\Gamma(c-a)\Gamma(b)}(-x)^{-a}F_4(a,a-c+1;d,a+1-b;y/x,1/x) + \frac{\Gamma(c)\Gamma(a-b)}{\Gamma(c-b)\Gamma(a)}(-x)^{-b}F_4(b,b-c+1;d,b+1-a;y/x,1/x).$$
(3.37)

Alternatively one can make use of a symmetry of F_4 and exchange (x, c) and (y, d) directly. As can be seen in fig. 3.2, a great part of the x-y-plane is still empty. Therefore we need another analytic continuation which is derived in Appendix B. The basic steps, however, are the same as above: We start directly with eq. (3.33) and analytically continue it again, but this time with another formula for ${}_2F_1$. Unfortunately we cannot rewrite the result into Appell's functions F_4 again and have to define two new series (eqs. (B.4) and (B.10)). The final result, eq. (B.12), is quite lengthy and consists of five single series.

3.3 Negative Dimensions Integration Method

Integration in negative dimensions sounds very abstract and naturally one asks what a negative dimension could mean. The short answer is: Physically it means nothing. The use of negative dimensions is merely a mathematical tool for calculating integrals. The method makes use of the mathematical concept of analytic continuation, which is applied on the number of dimensions. To fulfill certain constraints arising in this approach, the number of dimensions has to be negative in part, thus its name. In a wider sense NDIM can be compared to the method of dimensional regularization [54, 55]: Changing the value of the dimension away from four and permitting (intermediately) even non-integer values is nowadays commonly used. Continuing to negative values of the dimension goes just one step further. Nonetheless one should not confuse those two: Dimensional regularization is a tool for regularizing divergent integrals, whereas with NDIM one actually calculates integrals.

Originally NDIM was proposed by Halliday, Ricotta and Dunne [56, 57, 58, 59] who came up with the idea of using an analytic continuation of the dimension to negative values. A big advantage of NDIM is that the calculation is valid for arbitrary exponents in the integral. This is essential for this work, as the infrared exponents are non-integer numbers. In the literature, however, NDIM is not used very widely. Suzuki and Schmidt published several papers where they use NDIM, e.g. [60, 61, 62, 63, 64, 65], and there exists a detailed article by Anastasiou, Glover and Oleari [53], where they treat scalar one-loop Feynman integrals.

In this section I will demonstrate how NDIM is employed to calculate general one-loop Feynman diagrams. The calculation of tensor integrals can be done by standard methods, where one reduces the integrals to scalar ones. Alternatively one can use one of the two approaches given in [63]. I consider only massless integrals here. For the massive case I refer the reader to ref. [53]. The methods can be expanded to multi-loop calculations as well, confer for example ref. [66].

We want to calculate the following general scalar, one-loop n-point integral:

$$I_n(\{\nu_i\};\{p_i^2\}) \equiv \int d^d q \frac{1}{A_1^{\nu_1} \dots A_n^{\nu_n}}$$
 (3.38)

with the propagators A_i given by

$$A_1 = q^2,$$

$$A_i = \left(q + \sum_{j=1}^{i-1} p_j\right)^2, \qquad i \neq 1,$$
(3.39)

where q is the loop momentum and the p_i are external momenta which are all defined as incoming, see fig. 3.3. When comparing different references one has to be careful because the definition of the loop integral can differ with respect to the sign of the exponents ν_i .

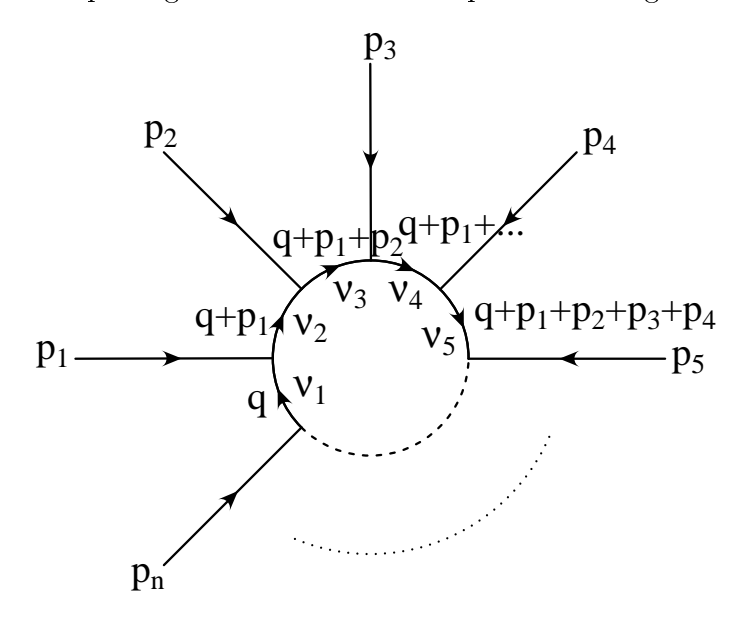


Figure 3.3: A general one-loop Feynman diagram with n legs. The external momenta are p_1 to p_n and q is the loop momentum. The ν_i denote the powers of the propagators.

First of all we employ a Schwinger parameter representation for the propagators,

$$\frac{1}{A^{\nu}} = \frac{1}{\Gamma(\nu)} \int_0^{\infty} dx \, x^{\nu - 1} e^{-x \, A},\tag{3.40}$$

which leads to

$$I_n(\{\nu_i\};\{p_i^2\}) = \int \mathfrak{D}x \int d^dk \, e^{-\sum_{i=1}^n x_i A_i}, \tag{3.41}$$

where $\int \mathfrak{D}x$ is defined as

$$\int \mathfrak{D}x \equiv \prod_{i=1}^{n} \frac{1}{\Gamma(\nu_i)} \int_0^\infty dx_i \, x_i^{\nu_i - 1},\tag{3.42}$$

but we will see shortly that it drops out of our calculation. The idea is now to proceed in two ways and compare the results at the end.

First we calculate the Gaussian integral directly after quadratic expansion of the exponent via

$$\int d^d q \, e^{-a \, q^2} = \left(\frac{\pi}{a}\right)^{\frac{d}{2}}.\tag{3.43}$$

This gives in the general case

$$I_n(\{\nu_i\};\{p_i^2\}) = \int \mathfrak{D}x \frac{1}{\mathcal{X}^{\frac{d}{2}}} \exp(\mathcal{Q}/\mathcal{X})$$
(3.44)

with

$$\mathcal{X} = \sum_{i=1}^{n} x_i,\tag{3.45}$$

$$Q = \sum_{i=1}^{n-1} \sum_{j=i+1}^{n} x_i x_j \left(\sum_{k=i}^{j-1} p_k\right)^2 = \sum_{i=1}^{r} Q_i.$$
 (3.46)

 \mathcal{X} and \mathcal{Q} can be derived from the quadratic expansion of the exponent in the integral. The calculation is mainly shifting the limits of sums and is very lengthy. As \mathcal{X} and \mathcal{Q} are used only for a general explanation in this chapter and not explicitly later on, the derivation is not given here. For now it is only important that the quantity \mathcal{Q} can be written as a sum of r terms denoted by \mathcal{Q}_i . The number r is derived from the number of possible combinations of x_i in eq. (3.46).

Alternatively we can do a Taylor expansion of eq. (3.41) which yields

$$I_n(\{\nu_i\}; \{p_i^2\}) = \int \mathfrak{D}x \int d^d q \sum_{n_1 \dots n_n = 0}^{\infty} \prod_{i=1}^n \frac{1}{n_i!} (-x_i A_i)^{n_i} =$$

$$= \int \mathfrak{D}x \sum_{n_1 \dots n_n = 0}^{\infty} \prod_{i=1}^n \frac{(-1)^{n_i} (x_i)^{n_i}}{n_i!} \int d^d q A_i^{n_i} =$$

$$= \int \mathfrak{D}x \sum_{n_1...n_n=0}^{\infty} \prod_{i=1}^n \frac{(-1)^{n_i} (x_i)^{n_i}}{n_i!} I_n(\{-n_i\}; \{p_i^2\}). \tag{3.47}$$

Eqs. (3.44) and (3.47) can be equated. Now we could expand eq. (3.44) in a Taylor series, but as we can see from a simple example, this leads to divergent integrals. The Taylor expansion of eq. (3.43) is

$$\int d^d q \, e^{-a \, q^2} = \int d^d q \sum_{n=0}^{\infty} \frac{a^n}{n!} (q^2)^n = \sum_{n=0}^{\infty} \frac{a^n}{n!} \int d^d q \, (q^2)^n. \tag{3.48}$$

As the solution nonetheless has to be $(\pi/a)^{\frac{d}{2}}$, we can "define"

$$\int d^d q \, (q^2)^n = \pi^{\frac{d}{2}} n! \delta_{n, -\frac{d}{2}} \tag{3.49}$$

to get the correct result. Because n has to be positive here, as it is a summation index, we "choose" d to be negative (and even) so this condition can be fulfilled. Assuming a negative d we can perform the Taylor expansion of eq. (3.44):

$$I_n(\{\nu_i\}; \{p_i^2\}) = \int \mathfrak{D}x \frac{1}{\mathcal{X}^{\frac{d}{2}}} \sum_{m=0}^{\infty} \frac{(\mathcal{Q}/\mathcal{X})^m}{m!} = \int \mathfrak{D}x \sum_{m=0}^{\infty} \frac{\mathcal{X}^{-m-\frac{d}{2}} \mathcal{Q}^m}{m!}.$$
 (3.50)

The last step, before a comparison of the two results is possible, is a multinomial expansion of the expressions \mathcal{X} and \mathcal{Q} in eq. (3.50). It is given by

$$(x_1 + \dots + x_m)^n = \sum_{k_1, \dots, k_m = 0}^{\infty} {n \choose k_1, \dots, k_m} x_1^{k_1} \dots x_m^{k_m} \qquad m \in \mathbb{N}, n \in \mathbb{N}_0$$
 (3.51)

$$\binom{n}{k_1, \dots, k_m} = \frac{n!}{k_1! \dots k_m!} \tag{3.52}$$

with the constraint

$$\sum_{i=1}^{m} k_i = n. (3.53)$$

It leads to

$$I_n(\{\nu_i\}; \{p_i^2\}) = \int \mathfrak{D}x \sum_{r_1, \dots, r_r=0}^{\infty} \sum_{s_1, \dots, s_n=0}^{\infty} \frac{\mathcal{Q}_1^{r_1}}{r_1!} \dots \frac{\mathcal{Q}_r^{r_r}}{r_r!} \frac{x_1^{s_1}}{s_1!} \dots \frac{x_n^{s_s}}{s_n!} (s_1 + \dots + s_n)!$$
 (3.54)

where the summation indices have to fulfill

$$r_1 + \ldots + r_r = m, (3.55)$$

$$s_1 + \ldots + s_n = -m - \frac{d}{2}. (3.56)$$

Finally we equate the two results. Because the Schwinger parameters x_i are independent we directly can compare the integrands of eqs. (3.47) and (3.54):

$$\sum_{n_1...n_n=0}^{\infty} \prod_{i=1}^{n} \frac{(-1)^{n_i} (x_i)^{n_i}}{n_i!} I_n(\{-n_i\}; \{p_i^2\}) =$$

$$= \sum_{r_1,...,r_r=0}^{\infty} \sum_{s_1,...,s_n=0}^{\infty} \frac{\mathcal{Q}_1^{r_1}}{r_1!} \dots \frac{\mathcal{Q}_r^{r_r}}{r_r!} \frac{x_1^{s_1}}{s_1!} \dots \frac{x_n^{p_n}}{p_n!} (p_1 + \dots + p_n)!.$$
(3.57)

When defining $\nu_i = -n_i$ the quantity to be calculated, $I_n(\{\nu_i\}; \{p_i^2\})$, is part of this equation and we have to match the powers of the x_i to get the final result. Doing so we get another set of constraints. Together with eqs. (3.55) and (3.56), which we combine to a single constraint,

$$r_1 + \ldots + r_r + s_1 + \ldots + s_n = -\frac{d}{2},$$
 (3.58)

we have a system of equations that has to be fulfilled by the summation indices. Note that d has to be negative here. This system of equations and

$$I_{n}(\{\nu_{i}\};\{p_{i}^{2}\}) =$$

$$= (-1)^{-\nu_{1}-\dots-\nu_{n}} \sum_{r_{1},\dots,r_{r}=0}^{\infty} \sum_{s_{1},\dots,s_{n}=0}^{\infty} \frac{Q_{1}^{r_{1}}}{r_{1}!} \dots \frac{Q_{r}^{r_{r}}}{r_{r}!} \frac{(-\nu_{1})! \dots (-\nu_{n})!}{s_{1}! \dots p_{s}!} (s_{1} + \dots + s_{n})! =$$

$$= (-1)^{-\nu_{1}-\dots-\nu_{n}} \sum_{r_{1},\dots,r_{r}=0}^{\infty} \sum_{s_{1},\dots,s_{n}=0}^{\infty} \frac{Q_{1}^{r_{1}}}{r_{1}!} \dots \frac{Q_{r}^{r_{r}}}{r_{r}!} \frac{\Gamma(1-\nu_{1}) \dots \Gamma(1-\nu_{n})}{\Gamma(1+s_{1}) \dots \Gamma(1+s_{n})} \Gamma(1+s_{1}+\dots+s_{n})$$

$$(3.59)$$

form the solution of our integral. It turns out that in the general case this system is under-determined and one or more summations are left. Before solving the system of equations we had r + n summation indices, where r was defined below eq. (3.46) and n is the number of legs, and n + 1 constraints, so that we end up with a series with r - 1 summation indices. Depending on what indices we choose to remain in the series we get different solutions. A few choices of indices, however, do not provide solutions. For each single solution we combine the Gamma functions to Pochhammer symbols and apply eq. (3.9) until we end up with hypergeometric functions. For these we determine their regions of convergence, which correspond to certain kinematic regions. For a result we have to sum up all series, which belong to the same region. As an alternative to calculating all

series we can do so in one region and then analytically continue them to the other ones.

The explanation of NDIM in this section was quite formal. The direct application for the calculation of the massless three-point integral in section 4.2.2 will show how NDIM works in practice.

4 Results

In [2] the infrared behavior of vertex functions in Landau gauge Yang-Mills theory was investigated in four dimensions. The goal of this chapter is a calculation in d dimensions. In the first section the infrared exponents of vertices are calculated via a naive power counting procedure and in the second one the ghost triangle, which is the first order of the skeleton expansion of the infrared dominant part of the three-gluon vertex, is calculated analytically using the full three-point integral in Euclidean space-time. Results for tensor components at special kinematic points are presented there. The d-dimensional calculation is supposed to determine whether the qualitative behavior of Green functions can be expected to be the same in two, three and four dimensions.

4.1 Naive Power Counting

4.1.1 The Infrared Behavior in Four Dimensions

I will shortly summarize the results from Alkofer, Fischer and Llanes-Estrada in [2]: Starting from the ghost-gluon vertex DSE the authors explain why the ghost-gluon vertex is bare in the infrared in Landau gauge (see section 2.1.2). Using this in the ghost DSE they get a relation between the infrared exponents of ghost and gluon propagator, expressed via one parameter κ . The value of κ is calculated in [23, 28] to be (93 – $\sqrt{1201}$)/98 \approx 0.595 in four dimensions, so the ghost propagator is divergent and the gluon propagator vanishing. They show that naive power counting is sufficient to determine the infrared behavior of vertex functions. In first order of the skeleton expansion of the three-gluon vertex they find the ghost-triangle to be the dominant part.

At the symmetric point (all squares of external momenta equal) they calculate the tensor components of the ghost triangle in the tensor basis of Celmaster and Gonsalves [67] by using an approximation that enables them to use the two-point integral [68].

They perform the power counting also for the four-gluon vertex and furthermore show that all higher orders of skeleton expansions yield the same infrared behavior. Thus, already the first term in the expansion yields the correct infrared exponent in the presence of only one external scale. The infrared exponent of a 2n-ghost-m-gluon amputated and connected Green function they determine to be $(n-m)\kappa$. At the end they demonstrate

that the running couplings from the ghost-gluon vertex, the three-gluon vertex and the four-gluon vertex have an infrared fixed point. All calculations were done in Landau gauge and Euclidean metric.

4.1.2 The Infrared Behavior in d Dimensions

In this section I will perform a naive power counting to get the infrared behavior of the propagators and the vertices in d dimensions. It will be shown that higher orders of the skeleton expansion also in dimensions other than four yield the same infrared exponent as the first order.



Figure 4.1: The DSE for the ghost propagator.

The starting point is the DSE of the ghost-gluon vertex. As was shown in section 2.1.2 the vertex stays bare in the infrared and does not renormalize. This is independent of the dimension and we use it in the DSE of the ghost propagator which is depicted in fig. 4.1. We make a power law ansatz for the dressing functions of gluon and ghost propagators,

$$Z(p^2) = A \cdot (p^2)^{\alpha}$$
 $G(p^2) = B \cdot (p^2)^{\beta},$ (4.1)

put these into the ghost DSE and compare the exponents of the external momentum p from both sides. For the integral on the right hand side one can use the two-point integral¹,

$$\int d^d q (q^2)^{\nu_1} ((q-p)^2)^{\nu_2} = (p^2)^{\frac{d}{2} + \nu_1 + \nu_2} \pi^{\frac{d}{2}} \frac{\Gamma(\frac{d}{2} + \nu_1) \Gamma(\frac{d}{2} + \nu_2) \Gamma(-\nu_1 - \nu_2 - \frac{d}{2})}{\Gamma(-\nu_1) \Gamma(-\nu_2) \Gamma(d + \nu_1 + \nu_2)}, \tag{4.2}$$

but at this point it is not even necessary because when we have only one external momentum, all momenta under the integral have to transform into that. Note at this point that A and B have dimension of $((momentum)^2)^{-\alpha}$ and $((momentum)^2)^{-\beta}$ respectively so that the dressing functions are dimensionless. The left hand side of the DSE, which consists only of the inverse dressed ghost propagator, is proportional to $(p^2)^{-\beta+1}$. The 1 comes from the p^2 in the definition of the ghost propagator, see eq. (A.3). On the right hand side we have $\frac{d}{2}$ from the integral, $\alpha-1$ from the gluon propagator, $\beta-1$ from the ghost propagator, $\frac{1}{2}$ from the bare ghost-gluon vertex and $\frac{1}{2}$ from the dressed ghost-gluon

¹One can calculate this formula with Feynman parameters or with NDIM. For two alternative derivations see Appendix B of [23].

vertex which we count as bare and is therefore proportional to the loop momentum:

$$1 - \beta = \frac{d}{2} + \alpha - 1 + \beta - 1 + \frac{1}{2} + \frac{1}{2}$$

$$\alpha = -2\beta + 2 - \frac{d}{2}.$$
(4.3)

Now we set $\beta = -\kappa$. In four dimensions we recover the well-known result $\alpha = 2\kappa$, but in d dimensions we have $\alpha = 2\kappa + 2 - \frac{d}{2}$. A comparison between different dimensions via κ is not possible directly, because κ has different values for different d [28, 29].

Now we have all the information we need for the next step, the calculation of the infrared exponent of the three-gluon vertex ($\rho_{2n,m}$ denotes the infrared exponent of a Green function with n ghost-antighost pairs and m gluons.):

• All dressed ghost-gluon vertices are replaced by bare ones, so their infrared exponent is

$$\rho_{2.1} = 0. (4.4)$$

They are proportional to p_{ν} , so we get $\frac{1}{2}$ from each.

• Infrared exponent of the gluon propagator:

$$\rho_{0,2} = 2\kappa + 2 - \frac{d}{2}.\tag{4.5}$$

We get $2\kappa + 1 - \frac{d}{2}$ from each.

• Infrared exponent of the ghost propagator:

$$\rho_{2,0} = -\kappa. \tag{4.6}$$

We get $-\kappa - 1$ from each.

A note on the term infrared exponent seems appropriate to avoid confusion: The infrared exponent is defined as the "additional" dependence on the external momentum. For example the ghost propagator consists of the dressing function $G(p^2)$ and $-\frac{1}{p^2}$. The infrared exponent is part of $G(p^2)$. Nevertheless $G(p^2)$ is dimensionless via B and the propagator has the dimension of $(momentum)^{-2}$. The same is valid for the gluon propagator and the ghost-gluon vertex has the dimension of momentum. The three-gluon vertex has also dimension of momentum as can be seen from the bare vertex, eq. (A.10). So in addition to the infrared exponent we always have to take into account the "normal" momentum dependence of the n-point function considered.

The first order of the skeleton expansion of the DSE for the three-gluon vertex is depicted in fig. 4.3. We start with the ghost triangle which is the infrared leading diagram. We have $\frac{d}{2}$ from the integral, $3(-\kappa-1)$ from the three ghost propagators and $\frac{3}{2}$ from the three

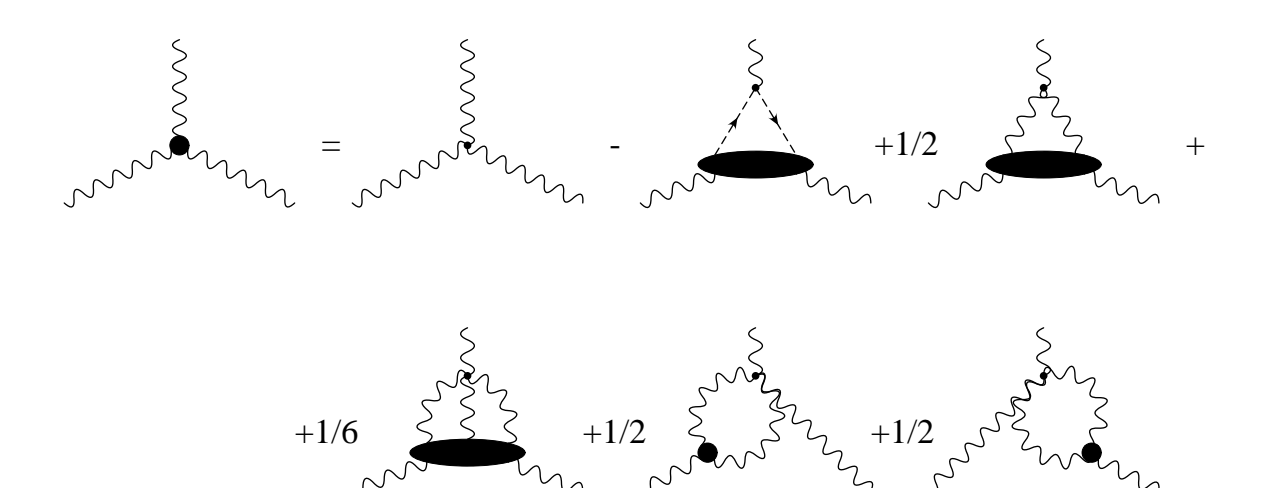


Figure 4.2: The complete DSE for the three-gluon vertex.

ghost-gluon vertices. We subtract $\frac{1}{2}$ to get the infrared exponent of the ghost triangle of the three-gluon vertex, denoted by $\rho_{0,3,gh-\Delta}$, where 0 stands for zero external ghosts, 3 for three external gluons and $gh - \Delta$ for ghost triangle:

$$\rho_{0,3,gh-\Delta} = \frac{d}{2} + 3(-\kappa - 1) + 3\frac{1}{2} - \frac{1}{2} = -3\kappa + \frac{d}{2} - 2. \tag{4.7}$$

Before calculating the infrared exponents of the other parts of the skeleton expansion we derive a general formula for Green functions in d dimensions assuming that the ghost triangle is the infrared dominant contribution. Therefore we define the following expressions (The bare four-gluon vertices are already included here as they appear in the first order of the skeleton expansion. Dressed four-gluon vertices, however, do not appear in first order and they are treated below.):

- *l*: number of loops
- m_i : number of internal gluons
- n_i : number of internal ghosts
- $v_{0,3}$: number of dressed three-gluon vertices
- $v_{0,3}^b$: number of bare three-gluon vertices
- $v_{2,1}$: number of ghost-gluon vertices, dressed or bare
- $v_{0.4}^b$: number of bare four-gluon vertices
- v: momentum dimension of the bare n-point function itself, for example $\frac{1}{2}$ for the three-gluon vertex

Now we are ready to set up the general formula. The task is straightforward as we only have to consider the following contributions:

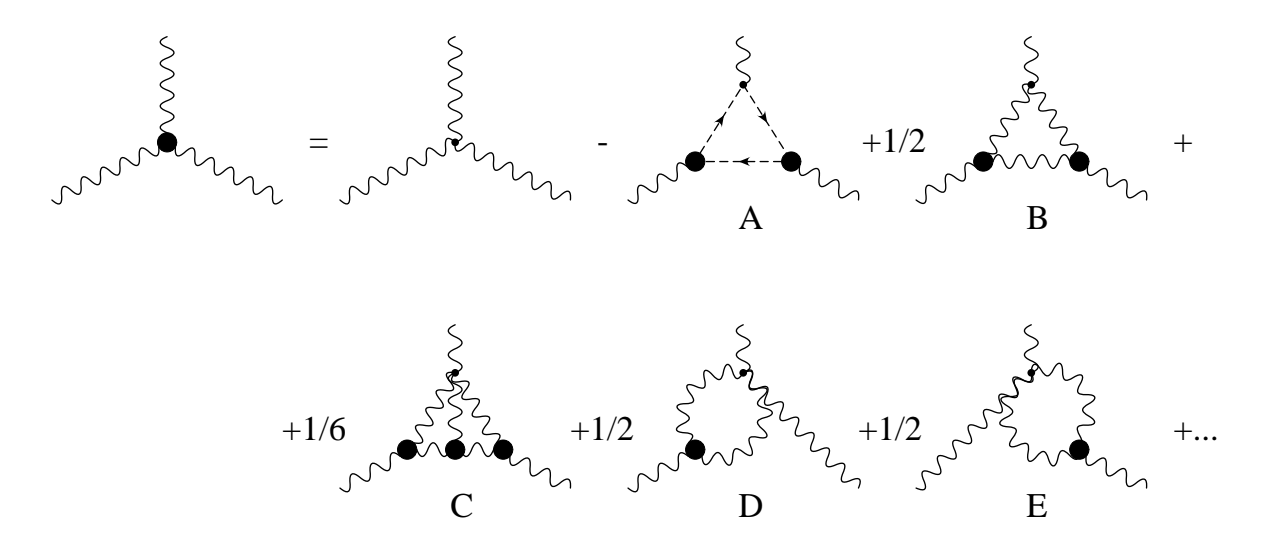


Figure 4.3: The first order of the skeleton expansion of the DSE for the three-gluon vertex.

- $\frac{d}{2}$ for every loop
- $\rho_{0,2} 1 = 2\kappa + 1 \frac{d}{2}$ for every internal gluon propagator
- $\rho_{2,0} 1 = -\kappa 1$ for every internal ghost propagator
- $\rho_{0,3} + \frac{1}{2} = -3\kappa + \frac{d}{2} \frac{3}{2}$ for every dressed three-gluon vertex
- $\frac{1}{2}$ for every ghost-gluon or bare three-gluon vertex
- 0 for every bare four-gluon vertex
- v is $\frac{1}{2}$ for the three-gluon and the ghost-gluon vertex, -1 for the propagators and 0 for the four-gluon vertex

Summing this up we get the infrared exponent of an arbitrary vertex v as

$$\rho_{v} = l \frac{d}{2} + m_{i} (2\kappa + 1 - \frac{d}{2}) + n_{i} (-\kappa - 1) + v_{0,3} (-3\kappa + \frac{d}{2} - \frac{3}{2}) + v_{0,3} \frac{1}{2} + v_{2,1} \frac{1}{2} + v_{0,4}^{b} \cdot 0 - v = (l - m_{i} + v_{0,3}) \frac{d}{2} + (2m_{i} - n_{i} - 3v_{0,3})\kappa + \frac{1}{2} (2m_{i} - 2n_{i} - 3v_{0,3} + v_{0,3}^{b} + v_{2,1} - 2v).$$
(4.8)

This formula we can process using some relations between the number of loops, the number of vertices and the number of propagators which can be found for example in [8]. At each vertex we have momentum conservation which leads to a delta function in the integral. Furthermore we have total momentum conservation, the delta function in front of the n-point function. So we add 1, for total momentum conservation, to the number of

all internal momenta, in our case $m_i + n_i$, and subtract the number of vertices, here $v_{0,4}^b + v_{0,3} + v_{0,3}^b + v_{2,1}$, to get the number of loop momenta:

$$l = m_i + n_i + 1 - (v_{0.4}^b + v_{0.3} + v_{0.3}^b + v_{2.1}). (4.9)$$

A second relation we get from comparing the number of vertices with the number of propagators. The task is simple: For every propagator type sum up the number of the vertices where it can start or end. Here we have to consider internal as well as external propagators, which are denoted by m and n for gluons and ghost-antighost-pairs respectively. In the case of gluons we get contributions from all vertices. For the ghosts only the ghost-gluon vertices contribute:

$$m + 2m_i = 4v_{0.4}^b + 3(v_{0.3} + v_{0.3}^b) + v_{2.1}, (4.10)$$

$$n + n_i = v_{2,1}. (4.11)$$

Note the different definition of m and n: The former denotes single gluons whereas the latter is the number of ghost-antighost pairs.

The last relation we need connects v, the momentum dimension of an arbitrary Green function, with m and n:

$$v = \frac{4 - (2n + m)}{2} = 2 - n - \frac{m}{2}. (4.12)$$

This formula is only valid for 2n+m>2, as the definition for bare and dressed propagators differs from that of higher Green functions.

Putting eqs. (4.9), (4.10), (4.11) and eq. (4.12) into eq. (4.8) we get

$$\rho_{2n,m} = \left(m_i + n_i + 1 - \left(v_{0,4}^b + v_{0,3} + v_{0,3}^b + v_{2,1} \right) - m_i + v_{0,3} \right) \frac{d}{2} + \\
+ \left(2m_i - n_i - 3v_{0,3} \right) \kappa + \frac{1}{2} \left(2m_i - 2n_i - 3v_{0,3} + v_{0,3}^b + v_{2,1} - (4 - 2n - m) \right) = \\
= \left(v_{2,1} - n + 1 - v_{0,4}^b - v_{0,3}^b - v_{2,1} \right) \frac{d}{2} + \\
+ \left(4v_{0,4}^b + 3(v_{0,3} + v_{0,3}^b) + v_{2,1} - m - (v_{2,1} - n) - 3v_{0,3} \right) \kappa + \\
+ \frac{1}{2} \left(4v_{0,4}^b + 3(v_{0,3} + v_{0,3}^b) + v_{2,1} - m - 2(v_{2,1} - n) - 3v_{0,3} \right) \kappa + \\
- 3v_{0,3} + v_{0,3}^b + v_{2,1} - 4 + 2n + m \right) = \\
= \left(-n + 1 - v_{0,4}^b - v_{0,3}^b \right) \frac{d}{2} + \left(4v_{0,4}^b + 3v_{0,3}^b - m + n \right) \kappa + \\
+ \left(2v_{0,4}^b + 2v_{0,3}^b + 2n - 2 \right). \tag{4.13}$$

This formula is still dependent on bare vertices. However, when considering different terms of the skeleton expansion of an n-point function, one easily sees that terms containing bare three- and four-gluon vertices are not the infrared dominant ones because contributions from these terms are

$$v_{0,3}^b(3\kappa - \frac{d}{2} + 2) \tag{4.14}$$

$$v_{0,4}^b(4\kappa - \frac{d}{2} + 2) \tag{4.15}$$

and thereby always positive. This means that diagrams that contain bare three- and four-gluon vertices have greater infrared exponents than diagrams without and the latter are the dominant ones in the infrared. So we can neglect the number of bare three- and four gluon vertices in the final formula for the infrared exponent of an n-point function:

$$\rho_{2n,m} = (1-n)\frac{d}{2} + (n-m)\kappa + (2n-2) = (n-m)\kappa + (1-n)(\frac{d}{2} - 2). \tag{4.16}$$

This formula was already derived independently by Fischer in 2006 [68].

Now we are in the position to derive the infrared exponents of the other diagrams of the three-gluon vertex DSE in fig. 4.3 via eq. (4.13). Diagram B contains one bare three-gluon vertex, so the infrared exponent is $(-3\kappa + \frac{d}{2} - 2) + (3\kappa - \frac{d}{2} + 2) = 0$. Diagrams C, D and E contain a bare four-gluon vertex and have therefore an infrared exponent of $(-3\kappa + \frac{d}{2} - 2) + (4\kappa - \frac{d}{2} + 2) = \kappa$. The results are the same as eqs. (13) in [2] independent of the dimension. Calculating the infrared exponent of the four-gluon vertex is now easy with eq. (4.16) at hand. We have m = 4, n = 0 and v = 0:

$$\rho_{0,4} = -4\kappa + \frac{d}{2} - 2. \tag{4.17}$$

An important part is still missing: What about higher orders in the skeleton expansion? From eq. (4.16) we can see immediately that higher orders terms have the same infrared behavior as the first term: Insertions which lead to higher orders only contribute with dressed vertices and propagators and these were all considered in the derivation of eq. (4.16). Such insertions are shown in fig. 4.4. Alternatively one can check this directly by counting the infrared exponents of these insertions (the $\frac{d}{2}$ stems from the additional loop integration that is necessary when inserting these diagrams):

A
$$(2\kappa + 1 - \frac{d}{2}) + 2(-\kappa - 1) + 2\frac{1}{2} + \frac{d}{2} = 0$$

B
$$2(2\kappa + 1 - \frac{d}{2}) + (-\kappa - 1) + (-3\kappa + \frac{d}{2} - \frac{3}{2}) + \frac{1}{2} + \frac{d}{2} = 0$$

C
$$3(2\kappa + 1 - \frac{d}{2}) + 2(-3\kappa + \frac{d}{2} - \frac{3}{2}) + \frac{d}{2} = 0$$

D
$$2(2\kappa + 1 - \frac{d}{2}) + (-4\kappa + \frac{d}{2} - 2) + \frac{d}{2} = 0$$

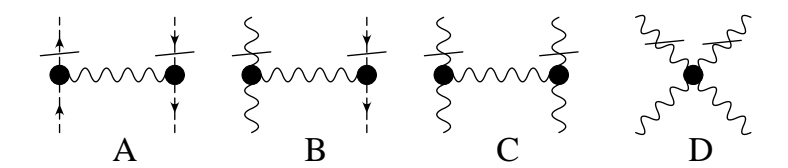


Figure 4.4: Insertions that generate higher orders in the skeleton expansion.

A remark on including the dressed four-gluon vertex in the derivation of eq. (4.16): In the DSE of the three-gluon vertex there are no dressed four-gluon vertices in the first order of the skeleton expansion. Higher orders, where dressed four-gluon vertices appear, can be achieved via updating a three- to a four-gluon vertex, but this does not change the infrared exponent. However, if one would like to include the dressed four-gluon vertex in the derivation of eq. (4.16), one can see straightforwardly that the result does not change: In eq. (4.8) we have the additional contribution $v_{0,4}(-4\kappa + \frac{d}{2} - 2)$, where it is important that the infrared exponent for the four-gluon vertex can also be calculated without eq. (4.16) via direct counting of the exponent of the ghost loop contribution in its DSE. The part proportional to $\frac{d}{2}$ cancels with the contribution from the four-gluon vertex to eq. (4.9). The contributions to the parts proportional to κ and $\frac{1}{2}$ cancel with the new part from eq. (4.10). Upon including contributions from dressed four-gluon vertices eqs. (4.9), (4.10) and (4.16) become

$$l = m_i + n_i + 1 - (v_{0,4}^b + v_{0,4} + v_{0,3} + v_{0,3}^b + v_{2,1}),$$

$$2m_i = 4(v_{0,4}^b + v_{0,4}) + 3(v_{0,3} + v_{0,3}^b) + v_{2,1} - m,$$

$$\rho_{2n,m} = (l - m_i + v_{0,3} + v_{0,4})\frac{d}{2} + (2m_i - n_i - 3v_{0,3} - 4v_{0,4})\kappa +$$

$$+ \frac{1}{2}(2m_i - 2n_i - 3v_{0,3} - 4v_{0,4} + v_{0,3}^b + v_{2,1} - 2v) =$$

$$= (n - m)\kappa + (1 - n)(\frac{d}{2} - 2).$$

$$(4.18)$$

Finally we can compare the infrared behavior of the Yang-Mills Green functions. In table 4.1 the complete momentum dependence of ghost and gluon propagator and the three-and four-gluon vertices are shown. One can see that the qualitative behavior does not change in different dimensions. Only the gluon propagator in two dimensions could be finite for one value of κ , in contrast to the other cases where it is infrared vanishing. Table 4.2 shows the infrared exponents.

Dimension		4	3		2	
κ		0.6	0.4	0.5	0.2	0
Ghost	$-\kappa - 1$	-1.6	-1.4	-1.5	-1.2	-1
Gluon	$2\kappa + 1 - \frac{d}{2}$	0.2	0.3	0.5	0.4	0
3-gluon	$-3\kappa + \frac{d}{2} - \frac{3}{2}$	-1.3	-1.2	-1.5	-1.1	-0.5
4-gluon	$-4\kappa + \frac{3}{2} - 2$	-2.4	-2.1	-2.5	-1.8	-1

Table 4.1: The dimension dependence of the infrared behavior of Yang-Mills Green functions.

Dimension		4	3		2	
κ		0.6	0.4	0.5	0.2	0
Ghost	$-\kappa$	-0.6	-0.4	-0.5	-0.2	0
Gluon	$2\kappa + 2 - \frac{d}{2}$	1.2	1.3	1.5	1.4	1
3-gluon	$-3\kappa + \frac{d}{2} - 2$	-1.8	-1.7	-2	-1.6	-1
4-gluon	$-4\kappa + \frac{\overline{d}}{2} - 2$	-2.4	-2.1	-2.5	-1.8	-1

Table 4.2: Infrared exponents of Yang-Mills Green functions in two, three and four dimensions.

4.2 Calculation of the Ghost Triangle

The results of the preceding section showed that the ghost triangle is the dominant part in the infrared also in two and three dimensions. Therefore, in this section I will calculate the ghost triangle of the three-gluon vertex DSE (see fig. 4.5) analytically using NDIM which was explained in section 3.3. One can keep the calculation general enough to end up with a formula for arbitrary exponents of the so-called three-point integral, so that this formula can also be used for other massless one-loop diagrams. Unfortunately the result is given in terms of Appell's series F_4 that does not converge in the Euclidean momentum region. For a solution in Euclidean space-time an analytic continuation of the series is required.

4.2.1 The Ghost Triangle

First of all we have to establish the integral we would like to calculate. Therefore we need the following (for details see Appendix A):

- The ghost propagator: $D_G^{ab}(k) = -\delta_{ab} \frac{G(k^2)}{k^2}$
- \bullet The bare ghost-gluon vertex: $G_{\mu}^{(bare)abc}(q,p)=i\,g\,f^{abc}\,q_{\mu}$

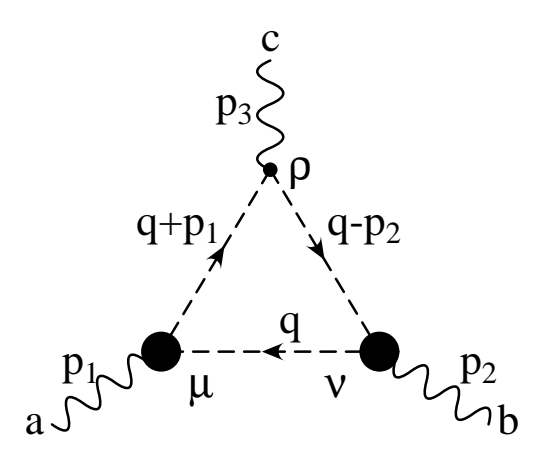


Figure 4.5: Momentum routing, Lorentz and color indices of the ghost triangle. Internal propagators are dressed and all gluon momenta are flowing inwards.

With the momentum routing depicted in fig. 4.5 and a minus sign from the fermion loop we get:

$$\Gamma_{\mu\nu\rho,gh-\Delta}^{abc}(p_{1},p_{2},p_{3}) =
= -\int \frac{d^{d}q}{(2\pi)^{d}} G_{\mu}^{ade}(q+p_{1},q) D_{G}^{fe}(q+p_{1}) G_{\rho}^{cfg}(q-p_{2},q+p_{1}) \times
\times D_{G}^{hg}(q-p_{2}) G_{\nu}^{bhi}(q,q-p_{2}) D_{G}^{di}(q) =
= -\int \frac{d^{d}q}{(2\pi)^{d}} i g f^{ade}(q+p_{1})_{\mu} (-\delta^{fe}) \frac{G((q+p_{1})^{2})}{(q+p_{1})^{2}} i g f^{cfg}(q-p)_{\rho} \times
\times (-\delta^{hg}) \frac{G((q-p_{2})^{2})}{(q-p_{2})^{2}} i g f^{bhi} q_{\nu} (-\delta^{di}) \frac{G(q^{2})}{q^{2}} =
= -i g^{3} \int \frac{d^{d}q}{(2\pi)^{d}} (q+p_{1})_{\mu} (q-p_{2})_{\rho} q_{\nu} f^{ade} f^{ceg} f^{bgd} \frac{G((q+p_{1})^{2})}{(q+p_{1})^{2}} \frac{G((q-p_{2})^{2})}{(q-p_{2})^{2}} \frac{G(q^{2})}{q^{2}}.$$
(4.21)

The color structure was evaluated with FeynCalc to be $-\frac{N_c}{2}f^{abc}$. We are interested in this integral at small external momenta p_1 , p_2 , and p_3 . Because of the denominators of the propagators the integral is then dominated by values of the loop momentum q also very small. Therefore we can put in the power law for the ghost propagator, see eq. (4.1), which is valid only for small momenta:

$$\Gamma_{\mu\nu\rho,gh-\Delta,IR}^{abc}(p_1,p_2,p_3) = i f^{abc} \frac{N_c B^3 g^3}{2} \int \frac{d^d q}{(2\pi)^d} (q+p_1)_{\mu} (q-p_2)_{\rho} q_{\nu} ((q+p_1)^2)^{-\kappa-1} ((q-p_2)^2)^{-\kappa-1} (q^2)^{-\kappa-1}.$$
(4.22)

4.2.2 Solution to the Massless Three-Point Integral

In this section I will calculate the formal solution of the scalar part of eq. (4.22). Therefore we denote a general three-point integral by

$$I(\nu_1, \nu_2, \nu_3; p_1, p_2, p_3) = \int d^d q ((q - p_2)^2)^{\nu_1} ((q + p_1)^2)^{\nu_2} (q^2)^{\nu_3}.$$
 (4.23)

As we saw in section 3.3 the integrals over the Schwinger parameters always cancel, so we start with the Gaussian integral

$$\int d^d q \, \exp\left(-x_1(q-p_2)^2 - x_2(q+p_1)^2 - x_3q^2\right) = \frac{\pi^{\frac{d}{2}}}{\phi^{\frac{d}{2}}} \exp\left(-\frac{1}{\phi}(x_1x_2p_3^2 + x_1x_3p_2^2 + x_2x_3p_1^2)\right). \tag{4.24}$$

 ϕ stands for $x_1 + x_2 + x_3$ and a quadratic expansion of the exponent was performed:

$$x_{3}q^{2} + x_{2}(q + p_{1})^{2} + x_{1}(q - p_{2})^{2} =$$

$$= (x_{1} + x_{2} + x_{3})q^{2} + 2q(x_{2}p_{1} - x_{1}p_{2}) + x_{2}p_{1}^{2} + x_{1}p_{2}^{2} =$$

$$= \phi(q + \frac{1}{\phi}(x_{2}p_{1} - x_{1}p_{2}))^{2} - \frac{1}{\phi}(x_{2}p_{1} - x_{1}p_{2})^{2} + x_{2}p_{1}^{2} + x_{1}p_{2}^{2} = \dots =$$

$$= \phi(q + \frac{1}{\phi}(x_{2}p_{1} - x_{1}p_{2}))^{2} + \frac{1}{\phi}(x_{1}x_{2}p_{3}^{2} + x_{1}x_{3}p_{2}^{2} + x_{2}x_{3}p_{1}^{2}). \tag{4.25}$$

Energy and momentum conservation in the form $p_3^2 = (p_1 + p_2)^2$ were employed.

The next steps are the Taylor expansion of the exponential in eq. (4.24) and the multinomial expansions² of ϕ and $(x_2x_3p_1^2 + x_1x_3p_2^2 + x_1x_2p_3^2)$:

$$\frac{\pi^{\frac{d}{2}}}{\phi^{\frac{d}{2}}} \sum_{n} \frac{1}{n!} \frac{(-1)^{n}}{\phi^{n}} (x_{2}x_{3}p_{1}^{2} + x_{1}x_{3}p_{2}^{2} + x_{1}x_{2}p_{3}^{2})^{n} =
= \pi^{\frac{d}{2}} \sum_{\{n_{i}\} = \left\{\frac{s_{1}, s_{2}, s_{3}, \\ r_{1}, r_{2}, r_{3}\right\}} \frac{(-1)^{n}}{n!} \frac{(-n - \frac{d}{2})!}{s_{1}! s_{2}! s_{3}!} \frac{n!}{r_{1}! r_{2}! r_{3}!} (x_{2}x_{3}p_{1}^{2})^{r_{1}} (x_{1}x_{3}p_{2}^{2})^{r_{2}} (x_{1}x_{2}p_{3}^{2})^{r_{3}} x_{1}^{s_{1}} x_{2}^{s_{2}} x_{3}^{s_{3}}. \tag{4.26}$$

The conditions from the multinomial expansions,

$$s_1 + s_2 + s_3 = -n - \frac{d}{2}, (4.27)$$

$$r_1 + r_2 + r_3 = n, (4.28)$$

²In the following all sums are understood to go from 0 to ∞ .

are combined to

$$s_1 + s_2 + s_3 + r_1 + r_2 + r_3 = -\frac{d}{2}. (4.29)$$

We also can make a Taylor expansion for the Gaussian integral in eq. (4.24):

$$\int d^{d}q \sum_{\nu_{1},\nu_{2},\nu_{3}} \frac{x_{1}^{\nu_{1}} x_{2}^{\nu_{2}} x_{3}^{\nu_{3}}}{\nu_{1}! \nu_{2}! \nu_{3}!} (-1)^{\nu_{1}+\nu_{2}+\nu_{3}} ((q-p_{2})^{2})^{\nu_{1}} ((q+p_{1})^{2})^{\nu_{2}} (q^{2})^{\nu_{3}} =
= \sum_{\nu_{1},\nu_{2},\nu_{3}} \frac{x_{1}^{\nu_{1}} x_{2}^{\nu_{2}} x_{3}^{\nu_{3}}}{\nu_{1}! \nu_{2}! \nu_{3}!} (-1)^{\nu_{1}+\nu_{2}+\nu_{3}} I(\nu_{1},\nu_{2},\nu_{3}; p_{1}, p_{2}, p_{3}).$$
(4.30)

By comparison of the exponents of the two eqs. (4.26) and (4.30) we get three additional constraints,

$$\nu_1 = s_1 + r_3 + r_2,
\nu_2 = s_2 + r_1 + r_3,
\nu_3 = s_3 + r_1 + r_2,$$
(4.31)

and the solution of the integral is

$$I(\nu_{1}, \nu_{2}, \nu_{3}; p_{1}, p_{2}, p_{3}) =$$

$$= \pi^{\frac{d}{2}} \sum_{\{n_{i}\}} (-1)^{r_{1}+r_{2}+r_{3}-\nu_{1}-\nu_{2}-\nu_{3}} \frac{(s_{1}+s_{2}+s_{3})!\nu_{1}!\nu_{2}!\nu_{3}!}{s_{1}!s_{2}!s_{3}!r_{1}!r_{2}!r_{3}!} (p_{1}^{2})^{r_{1}} (p_{2}^{2})^{r_{2}} (p_{3}^{2})^{r_{3}} =$$

$$= \pi^{\frac{d}{2}} \sum_{\{n_{i}\}} (-1)^{\frac{d}{2}} \frac{(s_{1}+s_{2}+s_{3})!\nu_{1}!\nu_{2}!\nu_{3}!}{s_{1}!s_{2}!s_{3}!r_{1}!r_{2}!r_{3}!} (p_{1}^{2})^{r_{1}} (p_{2}^{2})^{r_{2}} (p_{3}^{2})^{r_{3}}.$$

$$(4.32)$$

The system of linear equations consisting of eqs. (4.29) and (4.31) gives twelve non-vanishing solutions. They can be divided into three kinematic regions:

I:
$$\sqrt{p_2^2} + \sqrt{p_3^2} < \sqrt{p_1^2}$$

II:
$$\sqrt{p_1^2} + \sqrt{p_3^2} < \sqrt{p_2^2}$$

III:
$$\sqrt{p_1^2} + \sqrt{p_2^2} < \sqrt{p_3^2}$$

In the following we consider only region I, which means we keep as summation indices $\{s_2, s_3\}$, $\{s_2, r_3\}$, $\{s_3, r_2\}$ and $\{r_2, r_3\}$. It is not important which region we choose, because the three regions are connected via analytic continuations. In region I we get these solutions:

$$\begin{cases} \{s_2, s_3\} \colon & s_1 = -d - s_2 - s_3 - \nu_1 - \nu_2 - \nu_3 \\ & r_1 = -\frac{d}{2} - s_2 - s_3 - \nu_1 \\ & r_2 = \frac{d}{2} + s_2 + \nu_1 + \nu_3 \\ & r_3 = \frac{d}{2} + s_3 + \nu_1 + \nu_2 \end{cases}$$

$$\begin{cases} \{s_2, r_3\} \colon & s_1 = -\frac{d}{2} - s_2 - r_3 - \nu_3 \\ & s_3 = -\frac{d}{2} + r_3 - \nu_1 - \nu_2 \\ & r_1 = -s_2 - r_3 + \nu_2 \\ & r_2 = \frac{d}{2} + s_2 + \nu_1 + \nu_3 \end{cases}$$

$$\begin{cases} \{s_3, r_2\} \colon & s_1 = -\frac{d}{2} - s_3 - r_2 - \nu_2 \\ & s_2 = -\frac{d}{2} + r_2 - \nu_1 - \nu_3 \\ & r_1 = -s_3 - r_2 + \nu_3 \\ & r_3 = \frac{d}{2} + s_3 + \nu_1 + \nu_2 \end{cases}$$

$$\begin{cases} \{r_2, r_3\} \colon & s_1 = -r_2 - r_3 + \nu_1 \\ & s_2 = -\frac{d}{2} + r_2 - \nu_1 - \nu_3 \\ & s_3 = -\frac{d}{2} + r_3 - \nu_1 - \nu_2 \\ & r_1 = \frac{d}{2} - r_2 - r_3 + \nu_1 + \nu_2 + \nu_3 \end{cases}$$

For a result in region I we sum up the single solutions:

$$I(\nu_1, \nu_2, \nu_3; p_1, p_2, p_3) = I^{s_2, s_3} + I^{s_2, r_3} + I^{s_3, r_2} + I^{r_2, r_3}.$$

$$(4.33)$$

The single $I^{i,j}$, $i, j \in \{r_2, r_3, s_2, s_3\}$ are defined as the integral in eq. (4.32) with i and j as summation indices and the other indices determined by the solutions of the system of equations. I give the detailed calculation of I^{s_2,s_3} . The calculation of the other three cases is analog. The goal is to get I^{s_2,s_3} as a prefactor dependent on the momenta and the indices times a hypergeometric series.

$$\begin{split} I^{s_2,s_3}(\nu_1,\nu_2,\nu_3;p_1,p_2,p_3) &= \\ &= \pi^{\frac{d}{2}}(-1)^{\frac{d}{2}}\Gamma(1+\nu_1)\Gamma(1+\nu_2)\Gamma(1+\nu_3)\Gamma(1-\nu_1-\nu_2-\nu_3-d) \times \\ &\times \sum_{s_2,s_3} \frac{1}{s_2!s_3!} \left(\frac{p_2^2}{p_1^2}\right)^{s_2} \left(\frac{p_3^2}{p_1^2}\right)^{s_3} \frac{(p_1^2)^{-\frac{d}{2}-\nu_1}(p_2^2)^{\frac{d}{2}+\nu_1+\nu_3}(p_3^2)^{\frac{d}{2}+\nu_1+\nu_2}}{\Gamma(1-d-s_2-s_3-\nu_1-\nu_2-\nu_3)} \times \\ &\times \frac{1}{\Gamma(1-\frac{d}{2}-s_2-s_3-\nu_1)\Gamma(1+\frac{d}{2}+s_2+\nu_1+\nu_3)\Gamma(1+\frac{d}{2}+s_3+\nu_1+\nu_2)} = \\ &= \pi^{\frac{d}{2}}(-1)^{\frac{d}{2}} \frac{\Gamma(1+\nu_1)}{\Gamma(1-\frac{d}{2}-\nu_1)} \frac{\Gamma(1+\nu_2)}{\Gamma(1+\frac{d}{2}+\nu_1+\nu_2)} \frac{\Gamma(1+\nu_3)}{\Gamma(1+\frac{d}{2}+\nu_1+\nu_3)} \times \\ &\times (p_1^2)^{-\frac{d}{2}-\nu_1}(p_2^2)^{\frac{d}{2}+\nu_1+\nu_3}(p_3^2)^{\frac{d}{2}+\nu_1+\nu_2} \times \\ &\times \sum_{s_2,s_3} \frac{1}{s_2!s_3!} \left(\frac{p_2^2}{p_1^2}\right)^{s_2} \left(\frac{p_3^2}{p_1^2}\right)^{s_3} \frac{1}{(1-d-\nu_1-\nu_2-\nu_3,-s_2-s_3)} \times \end{split}$$

$$\times \frac{1}{(1 - \frac{d}{2} - \nu_{1}, -s_{2} - s_{3})(1 + \frac{d}{2} + \nu_{1} + \nu_{3}, s_{2})(1 + \frac{d}{2} + \nu_{1} + \nu_{2}, s_{3})} =$$

$$= \pi^{\frac{d}{2}}(-1)^{\frac{d}{2}}(1 - \frac{d}{2} - \nu_{1}, \frac{d}{2} + 2\nu_{1})(1 + \frac{d}{2} + \nu_{1} + \nu_{2}, -\frac{d}{2} - \nu_{1}) \times$$

$$\times (1 + \frac{d}{2} + \nu_{1} + \nu_{3}, -\frac{d}{2} - \nu_{1})(p_{1}^{2})^{-\frac{d}{2} - \nu_{1}}(p_{2}^{2})^{\frac{d}{2} + \nu_{1} + \nu_{3}}(p_{3}^{2})^{\frac{d}{2} + \nu_{1} + \nu_{2}}$$

$$\sum_{s_{2}, s_{3}} \frac{1}{s_{2}! s_{3}!} \left(\frac{p_{2}^{2}}{p_{1}^{2}}\right)^{s_{2}} \left(\frac{p_{3}^{2}}{p_{1}^{2}}\right)^{s_{3}} \times$$

$$\times \frac{(d + \nu_{1} + \nu_{2} + \nu_{3}, s_{2} + s_{3})(\frac{d}{2} + \nu_{1}, s_{2} + s_{3})}{(1 + \frac{d}{2} + \nu_{1} + \nu_{3}, s_{2})(1 + \frac{d}{2} + \nu_{1} + \nu_{2}, s_{3})} =$$

$$= \pi^{\frac{d}{2}}(p_{1}^{2})^{-\frac{d}{2} - \nu_{1}}(p_{2}^{2})^{\frac{d}{2} + \nu_{1} + \nu_{3}}(p_{3}^{2})^{\frac{d}{2} + \nu_{1} + \nu_{2}} \times$$

$$\times (\frac{d}{2} + \nu_{1}, -\frac{d}{2} - 2\nu_{1})(-\frac{d}{2} - \nu_{1} - \nu_{2}, \frac{d}{2} - \nu_{1})(-\frac{d}{2} - \nu_{1} - \nu_{3}, \frac{d}{2} + \nu_{1}) \times$$

$$\times F_{4}\left(d + \nu_{1} + \nu_{2} + \nu_{3}, \frac{d}{2} + \nu_{1}; 1 + \frac{d}{2} + \nu_{1} + \nu_{3}, 1 + \frac{d}{2} + \nu_{1} + \nu_{2}; \frac{p_{2}^{2}}{p_{1}^{2}}, \frac{p_{3}^{2}}{p_{1}^{2}}\right).$$

$$(4.34)$$

Successive use of eqs. (3.12), (3.3), (3.9) and (3.31) was made. Performing the same procedure for the other three cases one arrives at the final result:

$$\begin{split} I(\nu_{1},\nu_{2},\nu_{3};p_{1},p_{2},p_{3}) &= \pi^{\frac{d}{2}} \times \\ &\left\{ \frac{\Gamma(\frac{d}{2}+\nu_{1})\Gamma(-\frac{d}{2}-\nu_{1}-\nu_{3})\Gamma(-\frac{d}{2}-\nu_{1}-\nu_{2})(p_{1}^{2})^{-\frac{d}{2}-\nu_{1}}(p_{2}^{2})^{\frac{d}{2}+\nu_{1}+\nu_{3}}(p_{3}^{2})^{\frac{d}{2}+\nu_{1}+\nu_{2}}}{\Gamma(-\nu_{1})\Gamma(-\nu_{2})\Gamma(-\nu_{3})} \times \right. \\ &\left. \times F_{4}(d+\nu_{1}+\nu_{2}+\nu_{3},\frac{d}{2}+\nu_{1};1+\frac{d}{2}+\nu_{1}+\nu_{3},1+\frac{d}{2}+\nu_{1}+\nu_{2};\frac{p_{2}^{2}}{p_{1}^{2}},\frac{p_{3}^{2}}{p_{1}^{2}}) + \right. \\ &\left. + \frac{\Gamma(\frac{d}{2}+\nu_{1}+\nu_{3})\Gamma(\frac{d}{2}+\nu_{1}+\nu_{2})\Gamma(-\frac{d}{2}-\nu_{1}-\nu_{2}-\nu_{3})(p_{1}^{2})^{\frac{d}{2}+\nu_{1}+\nu_{2}+\nu_{3}}}{\Gamma(-\nu_{2})\Gamma(-\nu_{3})\Gamma(d+\nu_{1}+\nu_{2}+\nu_{3})} \times \right. \\ &\left. \times F_{4}(-\nu_{1},-\frac{d}{2}-\nu_{1}-\nu_{2}-\nu_{3};1-\frac{d}{2}-\nu_{1}-\nu_{3},1-\frac{d}{2}-\nu_{1}-\nu_{2};\frac{p_{2}^{2}}{p_{1}^{2}},\frac{p_{3}^{2}}{p_{1}^{2}}) + \right. \\ &\left. + \frac{\Gamma(\frac{d}{2}+\nu_{3})\Gamma(\frac{d}{2}+\nu_{1}+\nu_{2})\Gamma(-\frac{d}{2}-\nu_{1}-\nu_{3})(p_{1}^{2})^{\nu_{2}}(p_{2}^{2})^{\frac{d}{2}+\nu_{1}+\nu_{3}}}{\Gamma(-\nu_{1})\Gamma(-\nu_{3})\Gamma(d+\nu_{1}+\nu_{2}+\nu_{3})} \times \right. \\ &\left. \times F_{4}(\frac{d}{2}+\nu_{3},-\nu_{2};1+\frac{d}{2}+\nu_{1}+\nu_{3},1-\frac{d}{2}-\nu_{1}-\nu_{2};\frac{p_{2}^{2}}{p_{1}^{2}},\frac{p_{3}^{2}}{p_{1}^{2}}) + \right. \\ &\left. + \frac{\Gamma(\frac{d}{2}+\nu_{2})\Gamma(\frac{d}{2}+\nu_{1}+\nu_{3})\Gamma(-\frac{d}{2}-\nu_{1}-\nu_{2})(p_{1}^{2})^{\nu_{3}}(p_{3}^{2})^{\frac{d}{2}+\nu_{1}+\nu_{2}}}{\Gamma(-\nu_{1})\Gamma(-\nu_{2})\Gamma(d+\nu_{1}+\nu_{2}+\nu_{3})} \times \right. \\ &\left. \times F_{4}(\frac{d}{2}+\nu_{2})\Gamma(\frac{d}{2}+\nu_{1}+\nu_{3})\Gamma(-\frac{d}{2}-\nu_{1}-\nu_{2})(p_{1}^{2})^{\nu_{3}}(p_{3}^{2})^{\frac{d}{2}+\nu_{1}+\nu_{2}}}{\Gamma(-\nu_{1})\Gamma(-\nu_{2})\Gamma(d+\nu_{1}+\nu_{2}+\nu_{3})} \times \right. \\ \\ &\left. \times F_{4}(\frac{d}{2}+\nu_{1}+\nu_{2})\Gamma(\frac{d}{2}+\nu_{1}+\nu_{2}+\nu_{2})\Gamma(\frac{d}{2}+\nu_{1}+\nu_{2}+\nu_{2})\Gamma(\frac{d}{2}+\nu_{2}+\nu_{2}+\nu_{2}+\nu_{2}+\nu_{2}+\nu_{2}}{\Gamma(-\nu_{2}+\nu_$$

$$\times F_4(-\nu_3, \frac{d}{2} + \nu_2; 1 - \frac{d}{2} - \nu_1 - \nu_3, 1 + \frac{d}{2} + \nu_1 + \nu_2; \frac{p_2^2}{p_1^2}, \frac{p_3^2}{p_1^2}) \right\}. \tag{4.35}$$

Eq. (4.35) was already derived in [53, 69] via NDIM and an alternative method, but it was not mentioned that this representation is not convergent in the Euclidean momentum region as explained below.

4.2.3 Euclidean Region

Appell's series F_4 in eq. (4.35) is convergent for $\sqrt{\frac{p_2^2}{p_1^2}} + \sqrt{\frac{p_3^2}{p_1^2}} < 1$, but this is an inequality that cannot be fulfilled by Euclidean momenta as one can show from momentum and energy conservation, $p_1 + p_2 + p_3 = 0$:

$$p_1^2 = (-p_2 - p_3)^2 = p_2^2 + p_3^2 + 2p_2 \cdot p_3 = p_2^2 + p_3^2 + 2|p_2||p_3|\cos(\alpha).$$
 (4.36)

 α is the angle between p_2 and p_3 and its cosine ranges from -1 to +1 so that we get the following inequality $(x = \frac{p_2^2}{p_1^2}, y = \frac{p_3^2}{p_1^2})$:

$$p_2^2 + p_3^2 - 2|p_2||p_3| < p_1^2 < p_2^2 + p_3^2 + 2|p_2||p_3|$$

$$x + y - 2\sqrt{xy} < 1 < x + y + 2\sqrt{xy}.$$
(4.37)

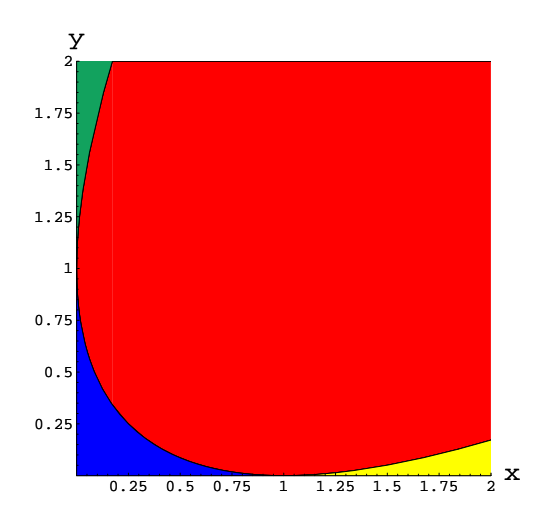


Figure 4.6: x and y are the ratios of the squared momenta. The Euclidean momentum region is in red, the region of convergence for the standard representation of Appell's series F_4 in blue. The green and yellow regions correspond to the series representations eqs. (3.35) and (3.37) respectively.

The values for which this inequality holds are depicted in red in fig. 4.6. The region of convergence for the series representation of Appell's series F_4 in eq. (4.35) is in blue. One can see clearly, that these two regions have no intersection and therefore Appell's series in eq. (4.35) does not converge.

In section 3.2.2 analytic continuations of Appell's series F_4 were considered. Equations eq. (3.35) and eq. (3.37), that continue the series from convergence around (0,0) to convergence around $(0,\infty)$ and $(\infty,0)$ respectively, fill the green and yellow regions in fig. 4.6. These green and yellow parts are the kinematic regions II and III. So we can alternatively use the analytic continuation formulas eq. (3.37) (region II) and eq. (3.35) (region III) instead of redoing the whole calculation for the other solutions. What is missing, is a continuation into the Euclidean region. This lengthy calculation can be found in Appendix B resulting in eq. (B.12), which is convergent in parts of the Euclidean region. The full solution of eq. (4.23) is then eq. (4.35) together with eq. (B.12) for Appell's functions F_4 .

4.2.4 Tensor Components

The result from the preceding chapter can be used to determine the tensor components of the ghost-triangle. Thereby the following quantity adopted from eq. (4.22) was calculated:

$$\Gamma_{\mu\nu\rho,gh-\Delta,IR}(p_1,p_2,p_3) = \frac{3}{2} \int \frac{d^dq}{(2\pi)^d} (q+p_1)_{\mu} (q-p_2)_{\rho} q_{\nu} ((q+p_1)^2)^{-\kappa-1} ((q-p_2)^2)^{-\kappa-1} (q^2)^{-\kappa-1}.$$
(4.38)

In the following this is written as $\Gamma_{\mu\nu\rho}$. The three-gluon vertex is composed of 14 tensor components:

$$\Gamma_{\mu\nu\rho} = \sum_{a} c_a \, \tau^a_{\mu\nu\rho}.\tag{4.39}$$

For calculating single tensor components c_a , one contracts on both sides with a basis tensor $\tau^b_{\mu\nu\rho}$,

$$\tau^b_{\mu\nu\rho}\Gamma_{\mu\nu\rho} = \sum_a c_a \, \tau^a_{\mu\nu\rho} \tau^b_{\mu\nu\rho},\tag{4.40}$$

which leads to a scalar integral on the left hand side that can be calculated. Doing so for all basis tensors one gets a system of equations, which has to be solved (except the basis is orthogonal, but this is not the case for the used bases).

For all calculations MATHEMATICA and the Mathematica package FEYNCALC were used. The difficulty in the implementation of eq. (B.12) are many special cases of the parameters that have to be considered. Such are for example occurrences of $\frac{\varepsilon}{(\varepsilon, m-n)}$, $\varepsilon \to 0$, where

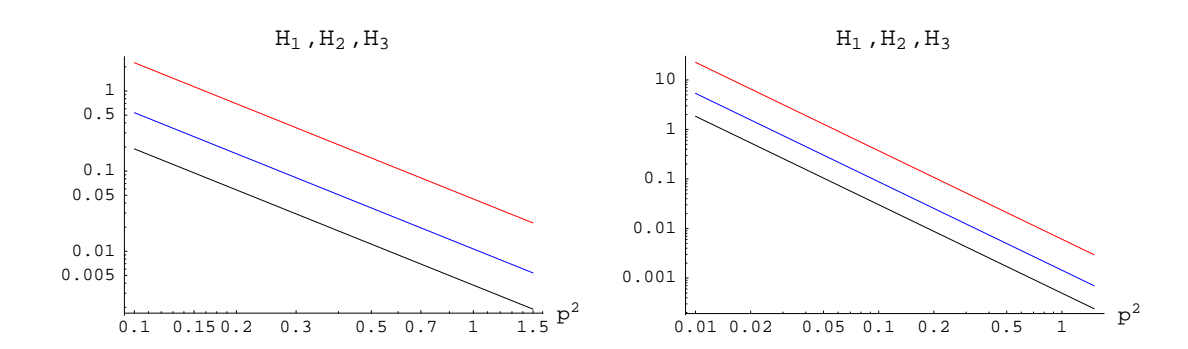


Figure 4.7: The three components of the three-gluon vertex at the symmetric point in three (left) and four dimensions. Black: H_1 . Blue: H_2 (negative). Red: H_3 . (Basis of Celmaster, Gonsalves [67]).

m and n are summation indices. Depending on the values of m and n this part is 0 or finite. Finally the code for evaluating three-point integrals was combined with a routine for extracting the tensor components. These were calculated for various kinematic points in three and four dimensions with the values of 0.4 and $\frac{93-\sqrt{1201}}{98}$ for κ respectively.

The simplest kinematics is at the symmetric point, for details see Appendix A. The symmetric point has the advantage that only three tensor components are necessary which are plotted in fig. 4.7 in a double-logarithmic plot. The slope of the three graphs was determined to be -1.78606 and -1.7, as expected, cf. table 4.2. The used basis is that of Celmaster and Gonsalves from [67]. The basis tensors are defined in Appendix A, eq. (A.22). For negative values the absolute values were taken³. No physical unit is given in the plots as we have no scale to determine one.

Another special kinematic point is the one with two momenta orthogonal to each other and the same magnitude, what corresponds to the point $(\frac{1}{2}, \frac{1}{2})$ in the x-y-plane of fig. 4.6. The tensor basis reduces to eleven tensors in this case, which are given in eq. (A.19) in Appendix A. This point is especially interesting as it is a favored point on the lattice where orthogonal configurations are very easy to achieve. The tensor components as defined in eq. (A.19) have an intrinsic dependence on the momentum. The reason for that are the basis tensors, which are not normalized. For example the basis tensor belonging to the function F_2 is proportional to $(p^2)^{\frac{5}{2}}$. As $\Gamma_{\mu\nu\rho}$ has to be proportional to momentum, the quantity $F_2 p^4$ was plotted to absorb the trivial scaling of the tensor. For the other functions according quantities were used in figs. 4.8, 4.9 and 4.10. The values of the slopes were determined to be the same as at the symmetric point.

Other special points in the x-y-plane of fig. 4.6 are for example $(\frac{1}{2}, 1)$ or $(1, \frac{1}{2})$. They also correspond to an orthogonal configuration of two momenta with the same magnitude.

³For which tensor components this applies is given in the description of the plots.

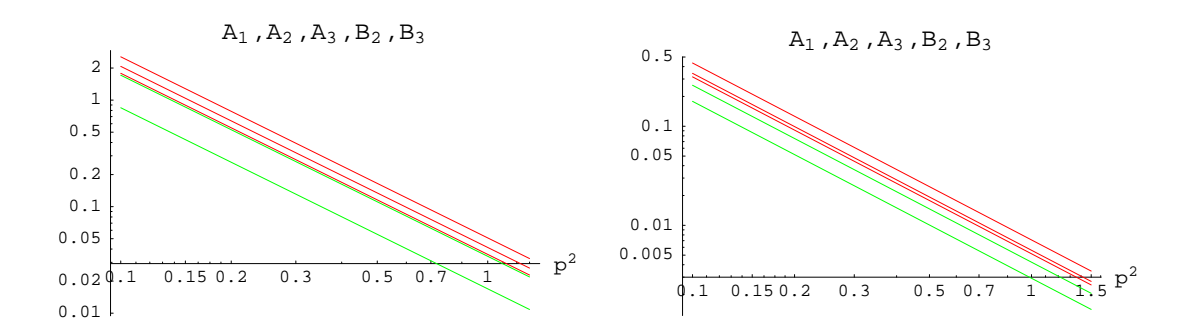


Figure 4.8: The components A_1 , A_2 , A_3 (red), B_2 and B_3 (green) of the three-gluon vertex in an orthogonal configuration in three (left) and four dimensions. A_1 , A_2 , A_3 and B_2 are negative.

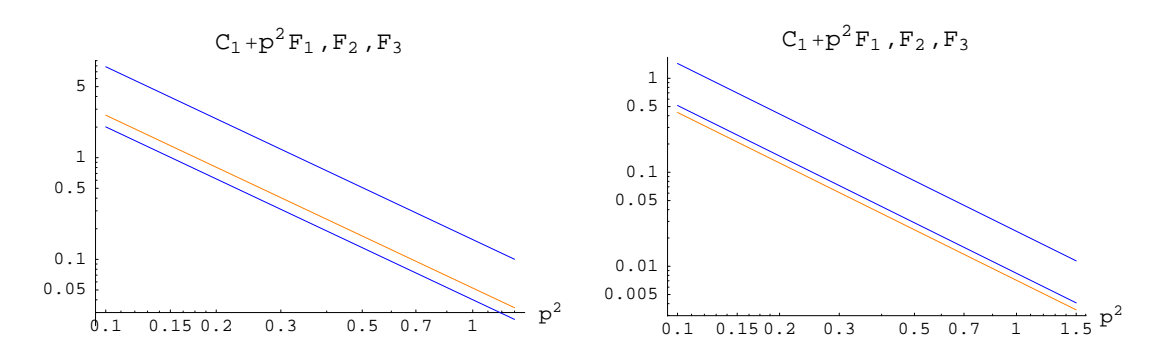


Figure 4.9: The components $C_1 + p^2 F_1$ (orange), F_2 and F_3 (blue) of the three-gluon vertex in an orthogonal configuration in three (left) and four dimensions. F_2 is negative.

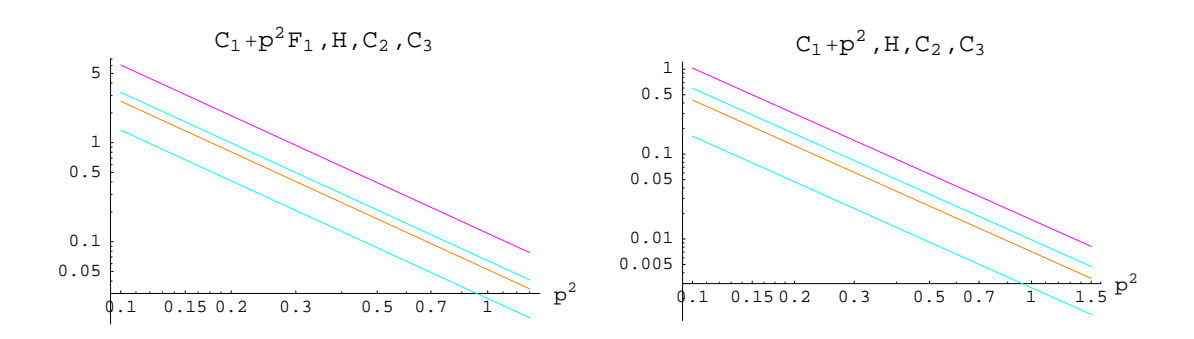


Figure 4.10: The components $C_1 + p^2 F_1$ (orange), H (magenta), C_2 and C_3 (cyan) of the three-gluon vertex in an orthogonal configuration in three (left) and four dimensions.

5 Conclusions

The main results of this thesis were presented in the preceding chapter. In the first part the power counting procedure devised by Alkofer, Fischer and Llanes-Estrada was extended to two and three dimensions. The expansion scheme used by them, the skeleton expansion, turned out to work also for two and three dimensions and the qualitative behavior of vertices and propagators proved to be very similar, i.e. in all three values of space-time dimension the ghost propagator and the gluon vertices show divergence, whereas the gluon propagator vanishes. The only exception is one of the two solutions for κ in two dimensions, which gives an infrared finite gluon propagator. The infrared exponents of propagators, three-gluon vertex and four-gluon vertex are listed in table 4.2. A comparison to Monte-Carlo simulations is not possible for the vertices yet, because the infrared region is not reached in neither value of space-time dimension. Hopefully this will improve in the near future and one will be able to compare the two methods.

A difficulty of the Dyson-Schwinger approach is finding ansätze for higher n-point functions and the results from [2] already provided useful input for this, as the required low momentum behavior for these ansätze is known. Within the extended power counting scheme presented here, applications are no longer restricted to four dimensions; for example the high-temperature limit of Landau gauge, cf. [29], is a three-dimensional theory. There is also a connection between Coulomb gauge in four and Landau gauge in three dimensions, and the results of this thesis can prove helpful when investigating this in more detail.

The analytic calculation of the ghost triangle showed that the three-gluon vertex behaves as predicted at low momenta (in first order of the skeleton expansion). A complete investigation of the whole Euclidean momentum region will provide more insight into the behavior at low energies, which can be used in further DSE studies. However, at the kinematic points considered in this thesis (the symmetric point and an orthogonal configuration of two momenta with the same magnitude), the behavior is as expected from naive power counting. In this work a method was presented how to deal with the known solution of the three-point integral, eq. (4.35), in Euclidean space-time by analytic continuation of Appells' function F_4 . The result, eq. (4.35) combined with eq. (B.12), may prove useful also in other areas.

Acknowledgements

Many people have contributed to this work by some means or other and I would like to take the chance to thank them here.

First of all I would like to thank my supervisor Dr. Reinhard Alkofer for inspiring me to work in such an interesting field and for his support.

I am very indebted to Dr. Kai Schwenzer, who also had a great share in the success of my work and with whom I had many long and fruitful discussions.

With Dr. Axel Maas and Dr. Christian S. Fischer I also enjoyed enlightening discussions for which I thank them.

I am grateful to Dipl.-Ing. Mag. Klaus Lichtenegger for listening to my stupid newbie questions and trying to answer them.

Furthermore I have to thank the foundation board of the Paul-Urban Stipendienstiftung who made it possible that I could present the results of this work under the title "Infrared Behavior of the Three-Gluon in d-dimensional Yang-Mills Theory" at the 45. Universitätswochen für Theoretische Physik in Schladming on the 28th of February 2007.

Thanks also to my friends, who were there when I needed distraction, and to Birgit for her understanding and love.

Finally I thank my parents, because without their ongoing support I would not be, where I am today.

A Conventions, Notations and Formulas

In books and articles about quantum field theory one often encounters different conventions and notations. These depend for example on the choice of metric, Minkowski or Euclidean, and there is also a certain freedom to define auxiliary quantities. In this work a consistent notation was attempted. Therefore I briefly summarize my notation, which is roughly the same as in [4] except a few minor changes. Throughout the whole thesis Landau gauge in Euclidean space-time was used. In diagrams blobs denote dressed propagators or vertices. Inner propagators are always dressed from section 2.2.3 onwards.

A.1 Propagators

The gluon propagator is denoted by a wiggly line and the ghost propagator by a dashed one, see fig. A.1.

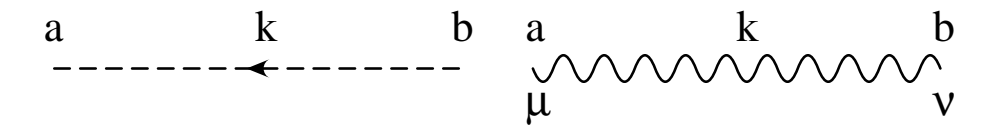


Figure A.1: Ghost and gluon propagator.

The color structure of both propagators is trivial, namely δ_{ab} . Therefore I will most of the time omit color indices. In general covariant gauge with the Lorenz gauge condition $\partial \cdot A = 0$ the gluon propagator has the following form:

$$D_{\mu\nu}^{ab}(k) = \delta_{ab} \frac{Z(k)}{k^2} \left[\delta_{\mu\nu} - (1 - \alpha) \frac{k_{\mu}k_{\nu}}{k^2} \right]. \tag{A.1}$$

The gauge fixing parameter α is defined by the gauging fixing term in the Lagrangian, $\mathcal{L}_{gf} = \frac{1}{2\alpha} (\partial_{\mu} A_{\mu}^{a})^{2}$, and Z(k) is the gluon dressing function. The bare gluon propagator is then

$$D_{\mu\nu}^{(bare)ab}(k) = \delta_{ab} \frac{1}{k^2} \left[\delta_{\mu\nu} - (1 - \alpha) \frac{k_{\mu} k_{\nu}}{k^2} \right]. \tag{A.2}$$

In Landau gauge α is 0. As an important consequence the gluon propagator is transverse, i.e. $k_{\mu}D_{\mu\nu}^{ab}(k) = 0$.

For the ghost propagator we have

$$D_G^{ab}(k) = -\delta_{ab} \frac{G(k^2)}{k^2}$$
 (A.3)

where $G(k^2)$ is the ghost dressing function, so that the bare propagator is

$$D_G^{(bare)ab}(k) = -\frac{\delta_{ab}}{k^2}. (A.4)$$

A.2 Vertices

In Yang-Mills theory there are only three primitively divergent vertices instead of the four in full QCD. These are the ghost-gluon vertex, the three-gluon vertex and the four-gluon vertex.

The ghost-gluon vertex couples a ghost-antighost-pair with one gluon, for details see section 2.1.2. It is interesting that in "ghost-free" gauges, as for example in axial gauge, DSEs not simplify as one would expect because of the non-existence of a ghost-gluon vertex. The reason is that the gluon propagator has an additional tensor component in axial gauge [4, 70].

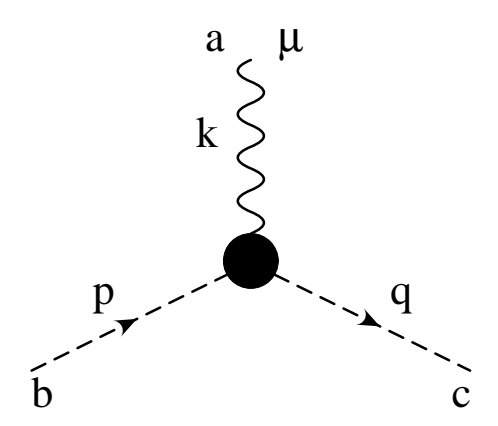


Figure A.2: The ghost-gluon vertex, the gluon momentum is ingoing.

The ghost-gluon vertex $G^{abc}_{\mu}(k;q,p)$ is here defined with incoming gluon momentum, denoted by the first momentum, and one outgoing and one incoming ghost momentum, denoted by the second and third momentum respectively. The color indices are mainly

suppressed so we define the following structure of the vertex functions to make the connection between colored and uncolored expressions clear:

$$G_{\mu}^{abc}(k;q,p) = (2\pi)^4 \delta(k+p-q) G_{\mu}^{abc}(q,p)$$
 (A.5)

$$G_{\mu}^{abc}(q,p) = f^{abc}G_{\mu}(q,p) \tag{A.6}$$

$$G_{\mu}(q,p) = i g q_{\nu} \widetilde{G}_{\mu\nu}(q,p). \tag{A.7}$$

For the bare vertex $\widetilde{G}_{\mu\nu}(q,p)$ becomes $\delta_{\mu\nu}$:

$$G_{\mu}^{(bare)abc}(q,p) = i g f^{abc} q_{\mu}. \tag{A.8}$$

For the three-gluon vertex we also define a structure similar to the one of the ghost-gluon vertex:

$$\Gamma^{abc}_{\mu\nu\rho}(p_1, p_2, p_3) = i g f^{abc}(2\pi)^4 \delta(p_1 + p_2 + p_3) \Gamma_{\mu\nu\rho}(p_1, p_2, p_3). \tag{A.9}$$

Here all momenta are defined to be ingoing and the color structure of the three-gluon vertex is proportional to f^{abc} as was verified on the lattice in ref. [71]. In this notation the tree-level expression is

$$\Gamma_{\mu\nu\rho}^{(bare)}(p_1, p_2, p_3) = \delta_{\mu\nu}(p_1 - p_2)_{\rho} + \delta_{\nu\rho}(p_2 - p_3)_{\mu} + \delta_{\mu\rho}(p_3 - p_1)_{\nu}. \tag{A.10}$$

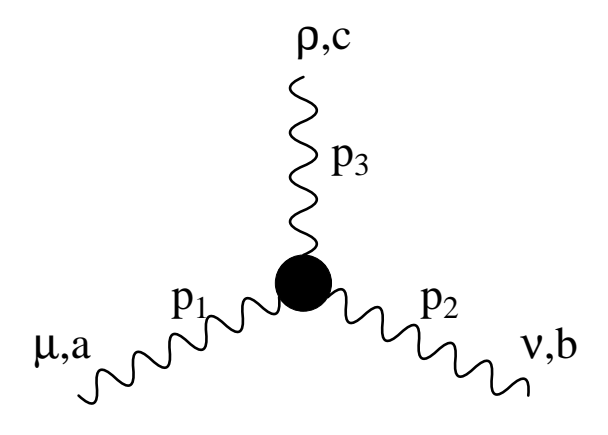


Figure A.3: The three-gluon vertex, all momenta are ingoing.

The tensor structure of the three-gluon vertex is quite complex. We have three momenta, p_1 , p_2 and p_3 , that are dependent on each other. Due to energy and momentum conservation the dependence reads

$$p_1 + p_2 + p_3 = 0. (A.11)$$

Out of two vectors and the metric tensor, $\delta_{\mu\nu}$, we can build fourteen tensors:

$$p_{1\mu}p_{1\nu}p_{1\rho}, p_{2\mu}p_{2\nu}p_{2\rho},$$

$$p_{1\mu}p_{1\nu}p_{2\rho}, p_{1\mu}p_{2\nu}p_{1\rho}, p_{2\mu}p_{1\nu}p_{1\rho},$$

$$p_{2\mu}p_{2\nu}p_{1\rho}, p_{2\mu}p_{1\nu}p_{2\rho}, p_{1\mu}p_{2\nu}p_{2\rho},$$

$$p_{1\mu}\delta_{\nu\rho}, p_{1\nu}\delta_{\mu\rho}, p_{1\rho}\delta_{\mu\nu},$$

$$p_{2\mu}\delta_{\nu\rho}, p_{2\nu}\delta_{\mu\rho}, p_{2\rho}\delta_{\mu\nu}.$$
(A.12)

Because of the total antisymmetry of the color part and the total symmetry of the threegluon vertex the Lorentz part has to be antisymmetric under the exchange of any two external momenta and the corresponding Lorentz indices. An often used basis is the so-called Ball-Chiu basis [72]. The tensors are split up into transverse and longitudinal parts. The transverse part is defined to be that part, that gives zero when contracted with an external momentum. It consists of four tensors.

$$\Gamma_{\mu\nu\rho}^{(t)}(p_{1}, p_{2}, p_{3}) = F_{3}(p_{1}^{2}, p_{2}^{2}; p_{3}^{2})(\delta_{\mu\nu}p_{1} \cdot p_{2} - p_{1_{\nu}}p_{2_{\mu}})\mathcal{B}_{\rho}^{3} + F_{1}(p_{2}^{2}, p_{3}^{2}; p_{1}^{2})(\delta_{\nu\rho}p_{2} \cdot p_{3} - p_{2_{\rho}}p_{3_{\nu}})\mathcal{B}_{\mu}^{1} + F_{2}(p_{3}^{2}, p_{1}^{2}; p_{2}^{2})(\delta_{\mu\rho}p_{3} \cdot p_{1} - p_{3_{\mu}}p_{1_{\rho}})\mathcal{B}_{\nu}^{2} + H(p_{1}^{2}, p_{2}^{2}, p_{3}^{2})(-\delta_{\mu\nu}\mathcal{B}_{\rho}^{3} - \delta_{\nu\rho}\mathcal{B}_{\mu}^{1} - \delta_{\mu\rho}\mathcal{B}_{\nu}^{2} + F_{1_{\rho}}p_{2_{\mu}}p_{3_{\nu}} - p_{1_{\nu}}p_{2_{\rho}}p_{3_{\mu}}), \tag{A.13}$$

where

$$\mathcal{B}_{\rho}^{3} = p_{1_{\rho}} p_{2} \cdot p_{3} - p_{2_{\rho}} p_{1} \cdot p_{3},$$

$$\mathcal{B}_{\mu}^{1} = p_{2_{\mu}} p_{3} \cdot p_{1} - p_{3_{\mu}} p_{2} \cdot p_{1},$$

$$\mathcal{B}_{\nu}^{2} = p_{3_{\nu}} p_{1} \cdot p_{2} - p_{1_{\nu}} p_{3} \cdot p_{2}.$$
(A.14)

The longitudinal part has ten tensors and reads

$$\Gamma_{\mu\nu\rho}^{(l)}(p_{1}, p_{2}, p_{3}) = A_{3}(p_{1}^{2}, p_{2}^{2}; p_{3}^{2})\delta_{\mu\nu}(p_{1} - p_{2})_{\rho} + A_{1}(p_{2}^{2}, p_{3}^{2}; p_{1}^{2})\delta_{\nu\rho}(p_{2} - p_{3})_{\mu} + A_{2}(p_{3}^{2}, p_{1}^{2}; p_{2}^{2})\delta_{\mu\rho}(p_{3} - p_{1})_{\nu} + B_{3}(p_{1}^{2}, p_{2}^{2}; p_{3}^{2})\delta_{\mu\nu}(p_{1} + p_{2})_{\rho} + A_{2}(p_{3}^{2}, p_{1}^{2}; p_{2}^{2})\delta_{\mu\rho}(p_{2} + p_{3})_{\mu} + A_{2}(p_{2}^{2}, p_{3}^{2}; p_{1}^{2})\delta_{\nu\rho}(p_{2} + p_{3})_{\mu} + A_{2}(p_{3}^{2}, p_{1}^{2}; p_{2}^{2})\delta_{\mu\rho}(p_{3} + p_{1})_{\nu} + A_{2}(p_{3}^{2}, p_{2}^{2}; p_{3}^{2})(p_{1\nu}p_{2\mu} - \delta_{\mu\nu}p_{1} \cdot p_{2})(p_{1} - p_{2})_{\rho} + A_{2}(p_{2}^{2}, p_{3}^{2}; p_{1}^{2})(p_{2\rho}p_{3\nu} - \delta_{\nu\rho}p_{2} \cdot p_{3})(p_{2} - p_{3})_{\mu} + A_{2}(p_{3}^{2}, p_{1}^{2}; p_{2}^{2})(p_{3\mu}p_{1\rho} - \delta_{\mu\rho}p_{3} \cdot p_{1})(p_{3} - p_{1})_{\nu} + A_{2}(p_{1}^{2}, p_{2}^{2}, p_{3}^{2})(p_{1\rho}p_{2\mu}p_{3\nu} + p_{1\nu}p_{2\rho}p_{3\mu}). \tag{A.15}$$

The following notation is quite common [72]:

$$\Gamma_{\mu\nu\rho}^{(t)}(p_{1}, p_{2}, p_{3}) = F(p_{1}^{2}, p_{2}^{2}; p_{3}^{2})(\delta_{\mu\nu}p_{1} \cdot p_{2} - p_{1\nu}p_{2\mu})\mathcal{B}_{\rho}^{3} + H(p_{1}^{2}, p_{2}^{2}, p_{3}^{2})(-\delta_{\mu\nu}B_{\rho}^{3} + H(p_{1}^{2}, p_{2}^{2}, p_{3}^{2})(-\delta_{\mu\nu}B_{\rho}^{3} + H(p_{1}^{2}, p_{2}^{2}, p_{3}^{2})) + \text{cycl. perm.},$$

$$\Gamma_{\mu\nu\rho}^{(l)}(p_{1}, p_{2}, p_{3}) = F(p_{1}^{2}, p_{2}^{2}; p_{3}^{2})\delta_{\mu\nu}(p_{1} - p_{2})_{\rho} + F(p_{1}^{2}, p_{2}^{2}; p_{3}^{2})\delta_{\mu\nu}(p_{1} + p_{2})_{\rho} + F(p_{1}^{2}, p_{2}^{2}; p_{3}^{2})(p_{1\nu}p_{2\mu} - \delta_{\mu\nu}p_{1} \cdot p_{2})(p_{1} - p_{2})_{\rho} + F(p_{1}^{2}, p_{2}^{2}; p_{3}^{2})(p_{1\nu}p_{2\mu} - \delta_{\mu\nu}p_{1} \cdot p_{2})(p_{1} - p_{2})_{\rho} + F(p_{1}^{2}, p_{2}^{2}; p_{3}^{2})(p_{1\nu}p_{2\mu}p_{3\nu} + p_{1\nu}p_{2\rho}p_{3\mu}) + \text{cycl. perm.}$$
(A.18)

The longitudinal part in this basis is actually not completely longitudinal because it is not orthogonal to the transverse part. It is defined as the remaining part of $\Gamma_{\mu\nu\rho}(p_1, p_2, p_3)$ after subtracting the transverse part and is constrained by the Ward-Takahashi identity. Another disadvantage of the Ball-Chiu basis is that the tree-level tensor, eq. (A.10), is not part of it. So a basis that has orthogonal tensors, which allows easy decomposition of the vertex into tensor components, including the tree-level tensor, would be the most convenient one.

The symmetry properties of the above scalar functions are as follows:

- Totally symmetric in all arguments: H
- Totally antisymmetric in all arguments: S
- Symmetric in the first two arguments: A_1 , A_2 , A_3 , C_1 , C_2 , C_3 , F_1 , F_2 , F_3
- Antisymmetric in the first two arguments: B_1 , B_2 , B_3

There are certain kinematic points at which the number of tensors reduces. One is the point with two momenta perpendicular to each other and the same magnitude. Let us assume that these two momenta are $p_2^2 = p_3^2 = p^2$. Then p_1 has to be $2p^2$. The scalar functions B_1 and S vanish because they are antisymmetric in p_2 and p_3 . As $p_2 \cdot p_3 = 0$ and $p_1 \cdot p_2 = p_1 \cdot p_3 = (p_2^2 - p_1^2 - p_3^2)/2 = -p^2$ the basis tensors then become

$$\begin{split} \Gamma^{(perp)}_{\mu\nu\rho}(p_1,p_2,p_3) = \\ F_3(2p^2,p^2;p^2)(-\delta_{\mu\nu}p^2 - p_{1_{\nu}}p_{2_{\mu}})p_{2_{\rho}}p^2 + \\ &+ (C_1(p^2,p^2;2p^2) + p^2\,F_1(p^2,p^2;2p^2))p_{2_{\rho}}p_{3_{\nu}}(p_{2_{\mu}} - p_{3_{\mu}}) + \\ &+ F_2(p^2,2p^2;p^2)(\delta_{\mu\rho}p^2 + p_{3_{\mu}}p_{1_{\rho}})p_{3_{\nu}}p^2 + \\ &+ H(2p^2,p^2,p^2)(-\delta_{\mu\nu}p_{2_{\rho}} + \delta_{\nu\rho}(p_{2_{\mu}} - p_{3_{\mu}}) + \delta_{\mu\rho}p_{3_{\nu}})p^2 + \end{split}$$

$$+ p_{1\rho}p_{2\mu}p_{3\nu} - p_{1\nu}p_{2\rho}p_{3\mu}) +$$

$$+ A_3(2p^2, p^2; p^2)\delta_{\mu\nu}(p_1 - p_2)_{\rho} +$$

$$+ A_1(p^2, p^2; 2p^2)\delta_{\nu\rho}(p_2 - p_3)_{\mu} +$$

$$+ A_2(p^2, 2p^2; p^2)\delta_{\mu\rho}(p_3 - p_1)_{\nu} +$$

$$+ B_3(2p^2, p^2; p^2)\delta_{\mu\nu}(p_1 + p_2)_{\rho} +$$

$$+ B_3(p^2, 2p^2; p^2)\delta_{\mu\rho}(p_3 + p_1)_{\nu} +$$

$$+ C_3(2p^2, p^2; p^2)(p_{1\nu}p_{2\mu} + \delta_{\mu\nu}p^2)(p_1 - p_2)_{\rho} +$$

$$+ C_2(p^2, 2p^2; p^2)(p_{3\mu}p_{1\rho} + \delta_{\mu\rho}p^2)(p_3 - p_1)_{\nu}. \tag{A.19}$$

Note that the tensors C_1 and F_1 , which come from the longitudinal and transverse part respectively, have merged into a single function $C_1 + p^2 F_1$.

A point with even less tensor components is the symmetric point, defined by

$$p_1^2 = p_2^2 = p_3^3 = p^2 (A.20)$$

which leads to

$$p_1 \cdot p_2 = p_2 \cdot p_3 = p_3 \cdot p_1 = -\frac{p^2}{2}.$$
 (A.21)

Only three basis tensors remain, which can be chosen according to [67] as

$$\Gamma_{\mu\nu\rho}^{(symm)}(p_1, p_2, p_3) = H_1(p^2) \left((p_1 - p_2)_{\rho} \delta_{\mu\nu} + (p_2 - p_3)_{\mu} \delta_{\nu\rho} + (p_3 - p_1)_{\nu} \delta_{\mu\rho} \right) + H_2(p^2) \frac{(p_2 - p_3)_{\mu} (p_3 - p_1)_{\nu} (p_1 - p_2)_{\rho}}{p^2} + H_3(p^2) \frac{p_{1\rho} p_{2\mu} p_{3\nu} - p_{1\nu} p_{2\rho} p_{3\mu}}{p^2}.$$
(A.22)

A.3 Gamma Function and Pochhammer Symbol

For easy reference I list certain relations of Gamma functions and Pochhammer symbols which can be useful for calculations with NDIM. Equations where the analytic continuation of the Pochhammer symbol is used require special attention if the second argument in the continued Pochhammer symbol is integer.

$$a \Gamma(a) = \Gamma(a+1) \qquad (a,b+c) = (a+b,c)(a,b) \qquad (A.23)$$

$$\Gamma(2a) = \frac{\Gamma(a)\Gamma(a+1/2)}{2^{1-2a}\sqrt{\pi}} \qquad (a,2b) = 2^{2b}(a/2,b)(1/2+a/2,b) \qquad (A.24)$$

$$\frac{\Gamma(a-n)}{\Gamma(a)} = (-1)^{-n} \frac{\Gamma(1-a)}{\Gamma(1-a+n)} \qquad (a,-n) = \frac{(-1)^{-n}}{(1-a,n)} \qquad (A.25)$$

$$\Gamma(a+b) = \Gamma(a)(a,b) \qquad \frac{1}{\Gamma(a+b)} = \frac{1}{\Gamma(a)(a,b)} \qquad (A.26)$$

$$\Gamma(a-b) = \Gamma(a)\frac{(-1)^b}{(1-a,b)} \qquad \frac{1}{\Gamma(a-b)} = \frac{(-1)^{-b}(1-a,b)}{\Gamma(a)} \qquad (A.27)$$

$$\Gamma(a+b+c) = \Gamma(a)(a+b,c)(a,b) \qquad \frac{1}{\Gamma(a+b+c)} = \frac{1}{\Gamma(a)(a+b,c)(a,b)} \qquad (A.28)$$

$$\Gamma(a+b-c) = \Gamma(a)(a,b)\frac{(-1)^c}{(1-a-b,c)} \qquad \frac{1}{\Gamma(a+b-c)} = \frac{(-1)^{-c}(1-a-b,c)}{\Gamma(a)(a,b)} \qquad (A.29)$$

$$\Gamma(a-b-c) = \Gamma(a)\frac{(-1)^{b+c}}{(1-a,b)(1-a-b,c)} \qquad \frac{1}{\Gamma(a-b-c)} = \frac{(-1)^{-b-c}(1-a,b)(1-a+b,c)}{\Gamma(a)} \qquad (A.30)$$

B Analytic Continuation of Appell's Function F_4 into the Euclidean Momentum Region

In this appendix I will derive the analytic continuation of Appell's function F_4 that was used in my calculations. It is more intricate than the well-known analytic continuation eq. (3.35) that is given as an example in section 3.2.2. The original derivation was done by Exton in [49]. In this appendix I will review it in more detail and correct a few misprints.

The first step is rewriting the original definition of F_4 in such a way that it contains the Gaussian hypergeometric series of one variable:

$$F_4(a,b;c,d;x,y) = \sum_{m=0}^{\infty} \frac{(a,m)(b,m)}{(c,m)} \frac{x^m}{m!} {}_2F_1(a+m,b+m;d;y).$$
 (B.1)

Now we use another analytic continuation of ${}_{2}F_{1}$, namely ((15.3.6) in [41])

$${}_{2}F_{1}(a,b;c;y) = \frac{\Gamma(c)\Gamma(c-a-b)}{\Gamma(c-a)\Gamma(c-b)} {}_{2}F_{1}(a,b;a+b-c+1;1-y) + \frac{\Gamma(c)\Gamma(a+b-c)}{\Gamma(a)\Gamma(b)} (1-y)^{c-a-b} {}_{2}F_{1}(c-a,c-b;c-a-b+1;1-y),$$
(B.2)

which is valid for $|\arg(1-y)| < \pi$. The condition is fulfilled naturally because we are only interested in real values of y. We put eq. (B.2) into eq. (B.1) and treat the two appearing terms separately. The first one will lead to a series which we call G according to the conventions of [49]. It is the easier one of the two emerging series:

$$\begin{split} \sum_{m=0}^{\infty} \frac{x^m}{m!} \frac{(a,m)(b,m)}{(c,m)} \frac{\Gamma(d)\Gamma(d-a-b-2m)}{\Gamma(d-a-m)\Gamma(d-b-m)} \sum_{n=0}^{\infty} \frac{(1-y)^n}{n!} \frac{(a+m,n)(b+m,n)}{(a+b+2m-d+1,n)} = \\ &= \frac{\Gamma(d)\Gamma(d-a-b)}{\Gamma(d-a)\Gamma(d-b)} \sum_{m,n=0}^{\infty} \frac{x^m}{m!} \frac{(1-y)^n}{n!} \frac{(a,m+n)(b,m+n)}{(c,m)(a+b+2m-d+1,n)} \frac{(d-a-b,-2m)}{(d-a,-m)(d-b,-m)} = \end{split}$$

$$= \frac{\Gamma(d)\Gamma(d-a-b)}{\Gamma(d-a)\Gamma(d-b)} \sum_{m,n=0}^{\infty} \frac{x^m}{m!} \frac{(1-y)^n}{n!} \frac{(a,m+n)(b,m+n)}{(c,m)} \frac{(1-d+a,m)(1-d+b,m)}{(1-d+a+b,2m+n)} = \frac{\Gamma(d)\Gamma(d-a-b)}{\Gamma(d-a)\Gamma(d-b)} G(a,b,1-d+a,1-d+b;1-d+a+b,c;x,1-y).$$
(B.3)

We have used eqs. (3.12) and (3.9) and the G series is defined as

$$G(a,b,c,d;e,f;x,y) = \sum_{m,n=0}^{\infty} \frac{x^m}{m} \frac{y^n}{n!} \frac{(a,m+n)(b,m+n)(c,m)(d,m)}{(e,2m+n)(f,m)}.$$
 (B.4)

The region of convergence for this series was calculated in section 3.1.5.

The second part is more intricate:

$$\sum_{m=0}^{\infty} \frac{x^m}{m!} \frac{(a,m)(b,m)}{(c,m)} \frac{\Gamma(d)\Gamma(a+b-d+2m)}{\Gamma(a+m)\Gamma(b+m)} (1-y)^{d-a-b-2m} \times \\ \times \sum_{n=0}^{\infty} \frac{(1-y)^n}{n!} \frac{(d-a-m,n)(d-b-m,n)}{(1+d-a-b-2m,n)} = \\ = \frac{\Gamma(d)\Gamma(a+b-d)}{\Gamma(a)\Gamma(b)} (1-y)^{d-a-b} \times \\ \times \sum_{m,n=0}^{\infty} \left(\frac{x}{(1-y)^2}\right)^m \frac{1}{m!} \frac{(1-y)^n}{n!} \frac{(a,m)(b,m)}{(c,m)} \frac{(a+b-d,2m)}{(a,m)(b,m)} \times \\ \times \frac{(d-a,n-m)}{(d-a,-m)} \frac{(d-b,n-m)}{(d-b,-m)} (-1)^n (a+b-d+2m,-n) = \\ = \frac{\Gamma(d)\Gamma(a+b-d)}{\Gamma(a)\Gamma(b)} (1-y)^{d-a-b} \times \\ \times \sum_{m,n=0}^{\infty} \left(\frac{x}{(1-y)^2}\right)^m \frac{(y-1)^n}{m!n!} \frac{(a+b-d,2m-n)(1+a-d,m)(1+b-d,m)}{(1+a-d,m-n)(1+b-d,m-n)(c,m)}.$$
(B.5)

We have made use of eqs. (3.12), (3.9) and (3.4). In this form the series is still not convergent in the Euclidean region and we need another analytical continuation. For this we rewrite eq. (B.5) into a form, that contains the generalized hypergeometric series ${}_{4}F_{3}$:

$$\begin{split} &\frac{\Gamma(d)\Gamma(a+b-d)}{\Gamma(a)\Gamma(b)}(1-y)^{d-a-b}\times\\ &\times\sum_{m,n=0}^{\infty}\left(\frac{x}{(1-y)^2}\right)^m\frac{(y-1)^n}{m!n!}\frac{(a+b-d,2m-n)(1+a-d,m)(1+b-d,m)}{(1+a-b,m-n)(1+b-d,m-n)(c,m)} =\\ &=\frac{\Gamma(d)\Gamma(a+b-d)}{\Gamma(a)\Gamma(b)}(1-y)^{d-a-b}\sum_{n=0}^{\infty}\frac{(y-1)^n}{n!}\frac{(a+b-d,n)}{1+a-d,n)(1+b-d,n)}\times\\ &\times\sum_{m=0}^{\infty}\left(\frac{x}{(1-y)^2}\right)^m\frac{(a+b-d-n,2m)(1+a-d,m)(1+b-d,m)}{m!(1+a-b-n,m)(1+b-d-n,m)(c,m)} =\\ &=\frac{\Gamma(d)\Gamma(a+b-d)}{\Gamma(a)\Gamma(b)}(1-y)^{d-a-b}\sum_{n=0}^{\infty}\frac{(y-1)^n}{n!}\frac{(-1)^n(d-a,n)(d-b,n)}{(1-a-b+d,n)}\times\\ &\times\sum_{m=0}^{\infty}\left(\frac{x}{(1-y)^2}\right)^m\frac{2^{2m}(\frac{a}{2}+\frac{b}{2}-\frac{d}{2}-\frac{n}{2},m)(\frac{1}{2}+\frac{a}{2}+\frac{b}{2}-\frac{d}{2}-\frac{n}{2},m)}{m!(1+a-b-n,m)(1+b-d-n,m)}\times\\ &\times\frac{(1+a-d,m)(1+b-d,m)}{(c,m)} =\\ &=\frac{\Gamma(d)\Gamma(a+b-d)}{\Gamma(a)\Gamma(b)}(1-y)^{d-a-b}\sum_{n=0}^{\infty}\frac{(1-y)^n}{n!}\frac{(d-a,n)(d-b,n)}{(1-a-b+d,n)}\times\\ &\times{}_{4F_3}\left(\frac{a}{2}+\frac{b}{2}-\frac{d}{2}-\frac{n}{2},\frac{1}{2}+\frac{a}{2}+\frac{b}{2}-\frac{d}{2}-\frac{n}{2},1+a-d,1+b-d;\frac{4x}{(1-y)^2}\right). \end{split}$$

Eqs. (3.4), (3.9) and (3.11) were used. The generalized hypergeometric series ${}_{4}F_{3}$ can be analytically continued with the Meijer-G function, which is in our case (eq. (5) on p. 208 in [48]):

$$G_{p,q}^{m,n}\left(x \middle| a_{1}, \dots, a_{p} \right) = \sum_{h=1}^{m} \frac{\prod_{j=1}^{m} \Gamma(b_{j} - b_{h}) \prod_{j=1}^{n} \Gamma(1 + b_{h} - a_{j})}{\prod_{j=m+1}^{q} \Gamma(1 + b_{h} - b_{j}) \prod_{j=n+1}^{p} \Gamma(a_{j} - b_{h})} x^{b_{h}} \times \left(1 + b_{h} - a_{1}, \dots, 1 + b_{h} - a_{p}; (-1)^{p-m-n} x\right) \qquad p < q \lor p = q \land |x| < 1.$$
(B.7)

The primed product excludes the expression $\Gamma(0)$ (when b=j), and the * stands for the one expression taken out as argument of ${}_{p}F_{q-1}$. A generalized hypergeometric series can

be expressed in terms of a Meijer-G function via (eq. (1) on page 215 in [48])

$$_{p}F_{q}(a_{1},\ldots,a_{p};b_{1},\ldots,b_{q};x) = \frac{\prod_{j=1}^{q}\Gamma(b_{j})}{\prod_{j=1}^{p}\Gamma(a_{j})}G_{q+1,p}^{p,1}\left(-\frac{1}{x}\begin{vmatrix}1,b_{1},\ldots,b_{q}\\a_{1},\ldots,a_{p}\end{pmatrix}\right).$$
 (B.8)

Our series ${}_{4}F_{3}$ from eq. (B.6) then becomes

$${}_{4}F_{3}(a,b,c,d;e,f,g;x) = \frac{\Gamma(e)\Gamma(f)\Gamma(g)}{\Gamma(a)\Gamma(b)\Gamma(c)\Gamma(d)}G_{4,4}^{4,1}\left(-\frac{1}{x}\begin{vmatrix} 1,e,f,g\\a,b,c,d \end{vmatrix}\right). \tag{B.9}$$

Inserting eq. (B.7) into eq. (B.9) is a bit tedious and MATHEMATICA was used for this task. It turns out, that two of the four expected ${}_4F_3$ vanish due to the appearance of $\Gamma(-n)$ in the denominator. This yields 0 because n is an integer. The two functions left are treated separately again. The calculation is tedious but straightforward: The goal is to rewrite the two sums again into a new double sum as above. For this we have to get rid of the $\frac{n}{2}$ that occur. We accomplish this by splitting the sum over n into two sums for even and odd n respectively. During the whole calculation eqs. (3.12), (3.9) and (3.4) are used. At the end we encounter a new series which Exton called K:

$$K(a,b,c,d;e,f,g,h;x,y) = \sum_{m,n=0}^{\infty} \frac{(a,m+n)(b,m+n)(c,m-n)(d,m-n)}{(e,m-n)(f,m-n)(g,m)(h,n)} \frac{x^m}{m!} \frac{y^n}{n!}.$$
(B.10)

It occurs four times (two times in each part from the splitting of the sum) and the total result of the analytic continuation is

$$\begin{split} L(a,b;c,d;\frac{(1-y)^2}{4x},\frac{x}{4}) &= \\ &= \frac{\Gamma(d)\Gamma(a+b-d)}{\Gamma(a)\Gamma(b)}\Gamma(c)\Gamma(\frac{1}{2})(-4x)^{\frac{d}{2}-\frac{a}{2}-\frac{b}{2}} \times \\ &\times \left\{ \frac{1}{\Gamma(\frac{a}{2}+\frac{b}{2}-\frac{d}{2}+\frac{1}{2})\Gamma(c-\frac{a}{2}-\frac{b}{2}+\frac{d}{2})} \times \\ &\times K\left(\frac{\frac{b}{2}-\frac{a}{2}+\frac{d}{2},\frac{a}{2}-\frac{b}{2}+\frac{d}{2},\frac{a}{2}+\frac{b}{2}-\frac{d}{2},\frac{a}{2}+\frac{b}{2}-c-\frac{d}{2}+1;\frac{(1-y)^2}{4x},\frac{x}{4}\right) + \\ &+ \frac{(d+a-b-1)(d-a+b-1)(-x)^{\frac{1}{2}}}{2(d-a-b+1)\Gamma(\frac{a}{2}+\frac{b}{2}-\frac{d}{2})\Gamma(c-\frac{a}{2}-\frac{b}{2}+\frac{d}{2}+\frac{1}{2})} \times \\ &K\left(\frac{\frac{b}{2}-\frac{a}{2}+\frac{d}{2}+\frac{1}{2},\frac{a}{2}-\frac{b}{2}+\frac{d}{2}+\frac{1}{2},\frac{a}{2}+\frac{b}{2}-\frac{d}{2}-\frac{1}{2},\frac{a}{2}+\frac{b}{2}-c-\frac{d}{2}+\frac{1}{2};\frac{(1-y)^2}{4x},\frac{x}{4}\right) + \\ &+ \frac{\Gamma(d)\Gamma(a+b-d)}{\Gamma(a)\Gamma(b)}\Gamma(c)\Gamma(-\frac{1}{2})(1-y)(-4x)^{\frac{d}{2}-\frac{a}{2}-\frac{b}{2}-\frac{1}{2}} \times \end{split}$$

$$\times \left\{ \frac{1}{\Gamma(\frac{a}{2} + \frac{b}{2} - \frac{d}{2})\Gamma(c - \frac{a}{2} - \frac{b}{2} + \frac{d}{2} - \frac{1}{2})} \times \left\{ \frac{b}{\Gamma(\frac{a}{2} + \frac{b}{2} - \frac{d}{2})}{(\frac{b}{2} - \frac{a}{2} + \frac{d}{2} + \frac{1}{2}, \frac{a}{2} - \frac{b}{2} + \frac{d}{2} + \frac{1}{2}, \frac{a}{2} + \frac{b}{2} - \frac{d}{2} + \frac{1}{2}, \frac{a}{2} + \frac{b}{2} - c - \frac{d}{2} + \frac{3}{2}; \frac{(1 - y)^{2}}{4x}, \frac{x}{4} \right) + \frac{(d + a - b)(d - a + b)(-x)^{\frac{1}{2}}}{2(d - a - b + 1)\Gamma(\frac{a}{2} + \frac{b}{2} - \frac{d}{2} - \frac{1}{2})\Gamma(c - \frac{a}{2} - \frac{b}{2} + \frac{d}{2})} \times \left\{ \frac{b}{2} - \frac{a}{2} + \frac{d}{2} + 1, \frac{a}{2} - \frac{b}{2} + \frac{d}{2} + 1, \frac{a}{2} + \frac{b}{2} - \frac{d}{2}, \frac{a}{2} + \frac{b}{2} - c - \frac{d}{2} + 1; \frac{(1 - y)^{2}}{4x}, \frac{x}{4} \right\} \right\}. \tag{B.11}$$

It is quite a lengthy expression and therefore Exton abbreviated it with $L(a, b, c, d; \frac{(1-y)^2}{4x}, \frac{x}{4})$. In contrast to the above defined G and K series, the combinations of x and y are fixed in the definition of L. This is caused by the appearance of x and y in the prefactors to the K series. L differs from the result given in [49]:

- The second term has an additional $\frac{1}{2}$.
- The third argument of the second K series has an additional $-\frac{1}{2}$.
- The second (-4x) has an additional $-\frac{1}{2}$ in the exponent.
- The fourth term has an additional $\frac{1}{2}$.

The corrections to reference [49] are red in eq. (B.11) for easier comparison. The final result for the Appell function is

$$F_4(a,b;c,d;x,y) = \frac{\Gamma(d)\Gamma(d-a-b)}{\Gamma(d-a)\Gamma(d-b)}G(a,b,1-d+a,1-d+b;1-d+a+b,c;x,1-y) + L(a,b,c,d;\frac{(1-y)^2}{4x},\frac{x}{4}).$$
(B.12)

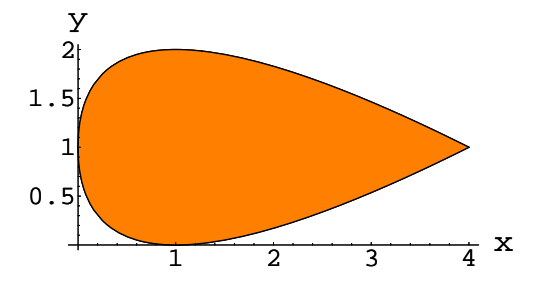


Figure B.1: The region of convergence for the K series.

To determine the region of convergence one can use the method of cancellation of parameters for K. Thereby one discovers that K reduces to the original definition of F_4 (set

c = e, d = f) and the region of convergence is

$$\sqrt{\frac{(1-y)^2}{4x}} + \sqrt{\frac{x}{4}} < 1. \tag{B.13}$$

This region is depicted in fig. B.1. The region of convergence for the G series can be derived via Horn's theorem, as was done in section 3.1.5. Comparing the two regions of convergence one sees that the K series is the limiting series.

There exist further analytic continuations with which one can cover the whole Euclidean momentum region. They are given in the appendix of [49] and correspond to the analytic continuations of the solutions in regions II and III, which were defined in section 4.2.2 below eq. (4.32). They are not necessary here, because we can always choose the ratios x and y in such a way, that the area in the rectangle defined by (0,0) and (1,1) is sufficient.

Bibliography

- [1] L. von Smekal, A. Hauck, and R. Alkofer, Ann. Phys. 267, 1 (1998), hep-ph/9707327.
- [2] R. Alkofer, C. S. Fischer, and F. J. Llanes-Estrada, Phys. Lett. B611, 279 (2005), hep-th/0412330.
- [3] A. Cucchieri, A. Maas, and T. Mendes, Phys. Rev. **D74**, 014503 (2006), hep-lat/0605011.
- [4] R. Alkofer and L. von Smekal, Phys. Rept. 353, 281 (2001), hep-ph/0007355.
- [5] C. S. Fischer, J. Phys. **G32**, R253 (2006a), hep-ph/0605173.
- [6] L. D. Faddeev and V. N. Popov, Phys. Lett. **B25**, 29 (1967).
- [7] S. Pokorski, Gauge Field Theories (Cambridge University Press, Cambridge, 1990).
- [8] L. H. Ryder, Quantum Field Theory (Cambridge University Press, Cambridge, 1996).
- [9] V. N. Gribov, Nucl. Phys. **B139**, 1 (1978).
- [10] P. van Baal, Nucl. Phys. **B369**, 259 (1992).
- [11] D. Zwanziger, Nucl. Phys. **B364**, 127 (1991).
- [12] D. Zwanziger, Nucl. Phys. **B399**, 477 (1993).
- [13] T. Kugo and I. Ojima, Prog. Theor. Phys. Suppl. 66, 1 (1979).
- [14] J. C. Taylor, Nucl. Phys. **B33**, 436 (1971).
- [15] W. J. Marciano and H. Pagels, Phys. Rept. **36**, 137 (1978).
- [16] W. Schleifenbaum, A. Maas, J. Wambach, and R. Alkofer, Phys. Rev. D72, 014017 (2005), hep-ph/0411052.
- [17] A. Cucchieri, T. Mendes, and A. Mihara, JHEP 12, 012 (2004), hep-lat/0408034.
- [18] A. Maas, A. Cucchieri, and T. Mendes (2006), hep-lat/0610006.
- [19] S. Mandelstam, Phys. Rev. **D20**, 3223 (1979).
- [20] N. Brown and M. R. Pennington, Phys. Rev. **D39**, 2723 (1989).
- [21] A. D. Worrall, Ph.d. thesis, University of Durham (1985).
- [22] A. Hauck, L. von Smekal, and R. Alkofer, Comput. Phys. Commun. 112, 149 (1998), hep-ph/9604430.

- [23] C. Lerche and L. von Smekal, Phys. Rev. **D65**, 125006 (2002), hep-ph/0202194.
- [24] A. Cucchieri, T. Mendes, and A. R. Taurines, Phys. Rev. D67, 091502 (2003), hep-lat/0302022.
- [25] C. S. Fischer, B. Gruter, and R. Alkofer, Ann. Phys. **321**, 1918 (2006), hep-ph/0506053.
- [26] C. S. Fischer, A. Maas, J. M. Pawlowski, and L. von Smekal (2007), to be published in Ann. Phys., hep-ph/0701050.
- [27] C. Lerche, Diploma thesis, University Erlangen, Nuremberg (2001 (in German)).
- [28] D. Zwanziger, Phys. Rev. **D65**, 094039 (2002), hep-th/0109224.
- [29] A. Maas, J. Wambach, B. Gruter, and R. Alkofer, Eur. Phys. J. C37, 335 (2004), hep-ph/0408074.
- [30] A. Maas, in preparation.
- [31] F. J. Dyson, Phys. Rev. **75**, 1736 (1949).
- [32] J. S. Schwinger, Proc. Nat. Acad. Sci. 37, 452 (1951a).
- [33] J. S. Schwinger, Proc. Nat. Acad. Sci. 37, 455 (1951b).
- [34] C. Itzykson and J.-B. Zuber, *Quantum Field Theory* (Dover Publications, Mineola, New York, 1980).
- [35] R. J. Rivers, Path Integrals Methods in Quantum Field Theory (Cambridge University Press, Cambridge, 1988).
- [36] C. D. Roberts and A. G. Williams, Prog. Part. Nucl. Phys. **33**, 477 (1994), hep-ph/9403224.
- [37] E. Eichten and F. Feinberg, Phys. Rev. **D10**, 3254 (1974).
- [38] M. Baker and C.-K. Lee, Phys. Rev. **D15**, 2201 (1977).
- [39] J. Bjorken and S. Drell, *Relativistische Quantenfeldtheorie* (Bibliographisches Institut, Mannheim, 1967).
- [40] H. M. Srivastava and P. W. Karlsson, Multiple Gaussian Hypergeometric Series (Ellis Horwood Limited, 1985).
- [41] M. Abramowitz and I. A. Stegun, *Handbook of Mathematical Functions* (Dover, New York, 1965).
- [42] C. B. Lang and N. Pucker, Mathematische Methoden in der Physik (Spektrum Akademischer Verlag, 1998).
- [43] A. P. Prudnikov, Y. A. Brychkov, and O. I. Marichev, *Integrals and Series*, vol. Volume 3: More special functions (Gordon and Breach Science, 1986).
- [44] P. Appell, C. R. Acad. Sci. Paris **90**, 296 (1880).

- [45] J. Horn, Math. Ann. **105**, 381 (1931).
- [46] J. Kampé de Fériet, C. R. Acad. Sci. Paris **173**, 401 (1921).
- [47] G. Lauricella, Rend. Circ. Mat. Palermo 7, 111 (1893).
- [48] A. Erdélyi, Higher Transcendental Functions, vol. 1 (McGraw-Hill, New York, 1953).
- [49] H. Exton, J. Phys. A 28, 631 (1994).
- [50] J. Horn, Math. Ann **34**, 544 (1889).
- [51] S. G. Krantz, Function theory of several complex variables (American Math. Soc., Providence, 2001).
- [52] I. S. Gradshteyn and I. M. Ryzhik, *Table of Integrals, Series, and Products* (Academic Press, London, 1980).
- [53] C. Anastasiou, E. W. N. Glover, and C. Oleari, Nucl. Phys. **B572**, 307 (2000), hep-ph/9907494.
- [54] G. 't Hooft and M. J. G. Veltman, Nucl. Phys. **B44**, 189 (1972).
- [55] C. G. Bollini and J. J. Giambiagi, Nuovo Cim. **B12**, 20 (1972).
- [56] I. G. Halliday and R. M. Ricotta, Phys. Lett. **B193**, 241 (1987).
- [57] G. V. Dunne and I. G. Halliday, Phys. Lett. **B193**, 247 (1987).
- [58] G. V. Dunne and I. G. Halliday, Nucl. Phys. **B308**, 589 (1988).
- [59] R. Ricotta, in J.J. Giambiagi Festschrift (ed. H. Falomir, 1990), p. 350.
- [60] A. T. Suzuki, E. S. Santos, and A. G. M. Schmidt, Eur. Phys. J. C26, 125 (2002a), hep-th/0205158.
- [61] A. T. Suzuki, E. S. Santos, and A. G. M. Schmidt (2002b), hep-ph/0210083.
- [62] A. T. Suzuki and A. G. M. Schmidt, J. Phys. **A33**, 3713 (2000), hep-th/0005082.
- [63] A. T. Suzuki and A. G. M. Schmidt, Eur. Phys. J. C10, 357 (1999), hep-th/9903076.
- [64] A. T. Suzuki and A. G. M. Schmidt, JHEP **09**, 002 (1997), hep-th/9709024.
- [65] A. T. Suzuki, A. G. M. Schmidt, and R. Bentin, Nucl. Phys. B537, 549 (1999), hep-th/9807158.
- [66] I. Gonzalez and I. Schmidt (2007), hep-th/0702218.
- [67] W. Celmaster and R. J. Gonsalves, Phys. Rev. **D20**, 1420 (1979).
- [68] C. S. Fischer, private communications.
- [69] E. E. Boos and A. I. Davydychev, Moscow Univ. Phys. Bull. **42N3**, 6 (1987).
- [70] K. Büttner and M. R. Pennington, Phys. Rev. **D52**, 5220 (1995), hep-ph/9506314.
- [71] P. Boucaud, J. P. Leroy, J. Micheli, O. Pene, and C. Roiesnel, JHEP 10, 017 (1998), hep-ph/9810322.
- [72] J. S. Ball and T.-W. Chiu, Phys. Rev. **D22**, 2550 (1980).